This is the accepted manuscript made available via CHORUS. The article has been published as:

Intertwined spin-orbital coupled orders in the iron-based superconductors

Morten H. Christensen, Jian Kang, and Rafael M. Fernandes

Phys. Rev. B **100**, 014512 — Published 15 July 2019

DOI: 10.1103/PhysRevB.100.014512

Intertwined spin-orbital coupled orders in the iron-based superconductors

Morten H. Christensen,* Jian Kang,† and Rafael M. Fernandes
School of Physics and Astronomy, University of Minnesota, Minneapolis, Minnesota 55455, USA
(Dated: May 24, 2019)

The underdoped phase diagram of the iron-based superconductors exemplifies the complexity common to many correlated materials. Indeed, multiple ordered states that break different symmetries but display comparable transition temperatures are present. Here, we argue that such a complexity can be understood within a simple unifying framework. This framework, built to respect the symmetries of the non-symmorphic space group of the FeAs/Se layer, consists of primary magnetically-ordered states and their vestigial phases that intertwine spin and orbital degrees of freedom. All vestigial phases have Ising-like and zero wave-vector order parameters, described in terms of composite spin order and exotic orbital-order patterns such as spin-orbital loop-currents, staggered atomic spin-orbit coupling, and emergent Rashba- and Dresselhaus-type spin-orbit interactions. Moreover, they host unusual phenomena, such as the electro-nematic effect, by which electric fields acts as transverse fields to the nematic order parameter, and the ferro-Néel effect, by which a uniform magnetic field induces Néel order. We discuss the experimental implications of our findings to iron-based superconductors and possible extensions to other correlated compounds with similar space groups.

I. INTRODUCTION

The complexity of the phase diagrams of correlated systems often challenges the notion of a unifying, simple framework to describe these fascinating systems. One example is that of the underdoped hole-doped cuprates: besides the mysterious pseudogap phenomenon, they display a plethora of ordered phases – incommensurate magnetism, charge order, nematicity, time-reversal symmetry-breaking order, and inversion symmetry-breaking order (for a recent review, see Ref. 1). As pointed out in Ref. 2, it is difficult to explain this richness solely in terms of independent, competing electronic orders. This led to proposals of a more fundamental type of ordered state, such as a pair-density wave [3–6], which simultaneously breaks several of the symmetries above-mentioned. In this scenario, the various broken-symmetry phases can be interpreted as vestigial orders that break only a subset of the symmetries of this "mother" state. To contrast with the standard case of competing orders and fine-tuned multicritical points, they have been dubbed intertwined orders [2, 7].

The phase diagram of underdoped iron-based superconductors seems relatively simpler compared to their copper-based counterparts [8–11]. Initial observations led to the concept of a typical phase diagram displaying two ordered normal states (besides superconductivity), namely, stripe magnetism and nematicity [12] (a notable exception is FeSe [13, 14], which we will discuss more later). One possible scenario is that these two ordered states have different microscopic origins [15–17]. However, early on, it was argued that the nematic state can be understood as a vestigial phase of the stripe magnetic state, as it breaks a subset of the symmetries broken by the latter – specifically, tetragonal symmetry [18–21]. In this scenario, stripe magnetism would be the "mother" phase of underdoped iron pnictides [22]. Nematic order is manifested in the electronic spectrum as orbital order involving the $3d_{xz}$, $3d_{yz}$, and $3d_{xy}$ Fe orbitals that form the low-energy electronic states. The vestigial nematic state in the iron pnictides is therefore a prime example of an intertwined spin-orbital coupled phase [23, 24], characterized by a composite spin order parameter and a simple (i.e. non-composite) orbital order parameter.

Analogously to the historical evolution of the "typical" phase diagram of the cuprates, more detailed experiments in the iron-based materials have recently unveiled a much more intricate underdoped phase diagram. In particular, besides stripe magnetism and nematicity, other types of magnetic order were observed to proliferate as optimal doping is approached [25]. These are magnetic configurations that do not break tetragonal symmetry [26–36], and have thus been dubbed C_4 magnetic phases. This phenomenon is observed quite broadly in hole-doped pnictides, and also in certain materials under pressure [34–37]. These observations called for revisiting the notion that stripe magnetism may be the "mother" phase of underdoped iron superconductors. A compelling scenario, put forward by several groups [20, 38–46], is that the C_4 phases are double-$\mathbf{Q}$ magnetic states, while the stripe phase is a single-$\mathbf{Q}$ magnetic state. Here, $\mathbf{Q}$ refers to two ordering vectors related by a 90° rotation; in the square unit cell containing one Fe atom only, $\mathbf{Q}_1 = (\pi, 0)$ and $\mathbf{Q}_2 = (0, \pi)$. In this scenario, all magnetically ordered phases are described in terms of two magnetic vector order parameters:

$$\mathbf{M}_1 = \begin{pmatrix} M_{1,x} \\ M_{1,y} \\ M_{1,z} \end{pmatrix}, \mathbf{M}_2 = \begin{pmatrix} M_{2,x} \\ M_{2,y} \\ M_{2,z} \end{pmatrix}. \quad (1)$$

Formally, $\mathbf{M}_a$ is the staggered Fe magnetization with mo-

* mchrist@umn.edu
† Present Address: National High Magnetic Field Laboratory, Florida State University, Tallahassee, Florida 32304, USA

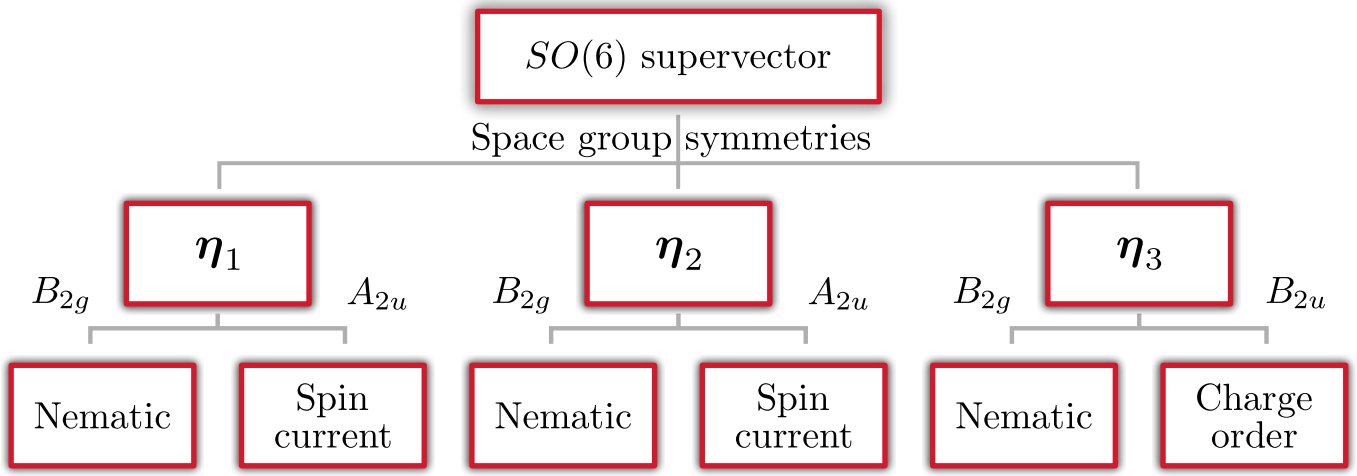

Figure 1. Schematic representation of the cascade of symmetry breakings leading to the emergence of intertwined orders in the iron-based superconductors. The starting point is the magnetic $SO(6)$ super-vector, presented in Eq. (3). Space-group symmetries only allow certain combinations of the super-vector components to order, giving rise to the primary magnetically ordered states $\boldsymbol{\eta}_i$. These, in turn, support different types of vestigial spin-orbital coupled phases, characterized by Ising-like, zero wave-vector order parameters that transform as the B_{2g}, A_{2u}, and B_{2u} irreducible representations of the tetragonal point group.

mentum $\mathbf{Q}_a$. One can then consider the "mother" order parameter as a hypothetical six-dimensional super-vector $\boldsymbol{\mathcal{M}} = (\mathbf{M}_1, \mathbf{M}_2)^T$. The symmetries of the square lattice only allow certain combinations of the six components of $\boldsymbol{\mathcal{M}}$ to condense, namely, one single-$\mathbf{Q}$ state (the stripe magnetic order) and two double-$\mathbf{Q}$ states (called spin-vortex crystal [33] and charge-spin density-wave [29]).

The single-$\mathbf{Q}$ phase breaks tetragonal symmetry and is therefore associated with a vestigial nematic phase. An important question is what types of vestigial orders can be associated with the double-$\mathbf{Q}$ magnetic phases. This question was partially addressed in Ref. 47, which proposed unusual vestigial phases that break translational and/or mirror symmetries, while preserving time-reversal symmetry. There is an important issue left unaddressed, however: what are the orbital-order patterns, if any, related to these vestigial phases? As discussed above, one of the hallmarks of nematicity is precisely its accompanying Fe-orbital order.

In this paper, we use group theory to determine the orbital ordering configurations of these vestigial phases, revealing a rich landscape of intertwined spin-orbital coupled phases. More than just an interesting extension of previous results, our work provides a powerful new framework to describe and predict possible ordered phases of underdoped iron-based superconductors, as well as their responses to external electromagnetic and strain fields. The key point is that the description of the magnetic degrees of freedom in terms of the order parameters $\mathbf{M}_1$ and $\mathbf{M}_2$ is inevitably incompatible with a description of the orbital degrees of freedom, due to the crystal symmetry of the FeAs (or FeSe) layer. More specifically, while the magnetic properties alone can be reasonably described in terms of a simplified unit cell containing only one Fe atom, the five $3d$ Fe-orbitals cannot.

The resolution to this conundrum is to note that the presence of a sizable spin-orbit coupling, as observed experimentally in most iron-based superconductors [48], ties the crystal symmetry properties of the spin degrees of freedom to those of the orbitals. Group-theoretical analysis of the space group of single-layered FeAs/Se superconductors ($P4/nmm$) then implies that the six components of $\boldsymbol{\mathcal{M}}$ should not be grouped in terms of two three-dimensional vectors with different wave-vectors, Eq. (1), but to three two-dimensional vectors with the same wave-vector [40, 41]:

$$\boldsymbol{\eta}_1 = \begin{pmatrix} M_{1,x} \\ M_{2,y} \end{pmatrix}, \boldsymbol{\eta}_2 = \begin{pmatrix} M_{1,y} \\ M_{2,x} \end{pmatrix}, \boldsymbol{\eta}_3 = \begin{pmatrix} M_{1,z} \\ M_{2,z} \end{pmatrix}. \quad (2)$$

In particular, while $\mathbf{M}_a$ lives in the artificial one-Fe square lattice unit cell ($a = 1, 2$), $\boldsymbol{\eta}_\alpha$ lives in the actual crystallographic unit cell of a single layer ($\alpha = 1, 2, 3$), containing two Fe atoms and two As/Se atoms. Because both wave-vectors $\mathbf{Q}_1 = (\pi, 0)$ and $\mathbf{Q}_2 = (0, \pi)$ of the 1-Fe Brillouin zone map onto the same wave-vector $\mathbf{Q}_M = (\pi, \pi)$ of the 2-Fe Brillouin zone, all $\boldsymbol{\eta}_\alpha$ have the same wave-vector, as seen in Fig. 2. Formally, they correspond to three two-dimensional irreducible representations of the FeAs single-layer space-group.

The important point is that any low-energy field-theory for the magnetic degrees of freedom should be formulated in terms of $\boldsymbol{\eta}_\alpha$, rather than $\mathbf{M}_a$, in contrast to what has been done extensively in the previous literature. Applying this formalism to classify the possible magnetically-driven vestigial orders, we find three distinct $\mathbf{Q} = 0$ orbitally-ordered states, characterized by Ising-like order parameters that are composite combinations of $\boldsymbol{\eta}_\alpha$ but simple (i.e. non-composite) combinations

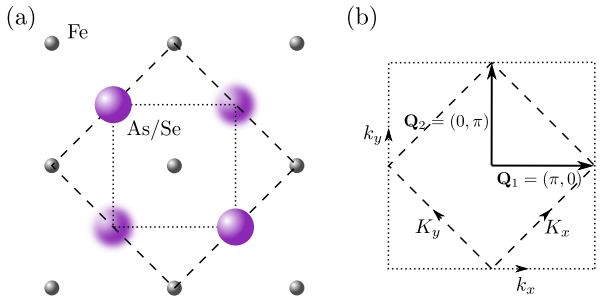

Figure 2. (a) Illustration of the 1-Fe (dotted square) and 2-Fe (dashed square) unit cells. To correctly capture the puckering of the As/Se atoms, two Fe atoms and two As/Se atoms are required in the unit cell. Here sharp purple spheres denote As/Se atoms above the Fe-layer while blurred purple spheres denote As/Se atoms below the Fe-layer. (b) Crystallographic 2-Fe Brillouin zone (dashed square) and idealized 1-Fe Brillouin zone (dotted square).

of orbital operators. They are:

1. The well-studied $\mathbf{Q} = 0$ nematic phase, whose Ising order parameter transforms as the B_{2g} irreducible representation of the tetragonal group. This is the vestigial phase of the stripe magnetic state. The corresponding orbital order configuration is a mixture of onsite and bond d_{xz}/d_{yz} ferro-orbital order, as well as d_{xy} bond order. Structurally, this order couples to an acoustic phonon mode, and is thus accompanied by an orthorhombic lattice distortion. Its conjugate field is shear strain along the Fe-Fe bonds.

2. A $\mathbf{Q} = 0$ ordered phase whose Ising order parameter transforms as the B_{2u} irreducible representation of the tetragonal group. This is the vestigial phase of the charge-spin density-wave state. The corresponding orbital order configuration is a combination of intra-unit-cell staggered charge order on the d_{xy} orbitals and a intra-unit-cell "staggered spin-orbit coupling" ordering involving the d_{xz}/d_{yz} orbitals. This ordered state does not couple to any new atomic displacements, but it does remove the spin-degeneracy of the bands, giving rise to spontaneously generated Dresselhaus-type and Rashba-type spin-orbit terms. For simplicity, we refer to this phase as the charge-ordered state. Its conjugate field is a combination of an electric field perpendicular to the FeAs-layer and shear strain along the Fe-As bonds.

3. A $\mathbf{Q} = 0$ ordered phase whose Ising order parameter transforms as the A_{2u} irreducible representation of the tetragonal group. This is the vestigial phase of the spin-vortex crystal state. The corresponding orbital order configuration is a mixture of staggered spin-current patterns involving the d_{xy} orbitals and a mirror-symmetry breaking ordering involving the d_{xz}/d_{yz} orbitals. This type of order couples to an optical phonon mode, whose softening however does not lead to any new atomic displacements. Similarly to the B_{2u} Ising order, it also removes the spin-degeneracy of the bands, triggering the appearance of Dresselhaus-type and Rashba-type spin-orbit terms. For simplicity, we refer to this phase as the spin-current state. Its conjugate field is an electric field perpendicular to the FeAs-layer.

A summary of the framework derived here, including the primary magnetic states and their vestigial phases is shown in Fig. 1. Because these three vestigial phases are not independent, but connected by transformations in the two-dimensional internal spaces of the $\boldsymbol{\eta}_\alpha$ order parameters, they can act as "transverse fields" to each other [49]. This opens the possibility of using, for instance, an electric field to induce the spin-current vestigial order, which can then be employed to tune the nematic phase transition. This rather unusual effect, which we dub *electro-nematic effect*, is intimately connected to the intertwined character of phases that break completely different symmetries.

The same formalism can be used to investigate how the vestigial phases respond to external fields, such as a magnetic field $\mathbf{H}$. In the nematic phase, the field simply induces a finite magnetization, as expected for a standard paramagnet. However, in the charge-ordered and spin-current states, the field $\mathbf{H}$ also induces a finite Néel magnetization $\mathbf{N}$, despite the absence of any long-range magnetic order. In the charge-ordered state, $\mathbf{N} \parallel \mathbf{H}$, resulting in a ferrimagnetic spin configuration, whereas in the spin-current state we find that an in-plane magnetic field induces a canted spin configuration for $\mathbf{H} \parallel \hat{\mathbf{x}}$ or $\mathbf{H} \parallel \hat{\mathbf{y}}$, and a ferrimagnetic configuration if $\mathbf{H}$ is applied along the diagonal direction of the 1-Fe unit cell. This effect, which we dub *ferro-Néel effect*, shows the nontrivial character of these vestigial paramagnetic phases, and can be used to identify these exotic spin-orbit coupled vestigial states.

This paper is organized as follows: In Sec. II we discuss how vestigial phases arise in the iron-based systems. We argue that the fundamental degrees of freedom are given by Eq. (2), and write down the field theory invariant under the space-group symmetries of the FeAs/Se layer. We demonstrate that vestigial phases can arise in the paramagnetic state, and are characterized by composite spin order. In Sec. III, we derive the electronic orders arising as consequences of the vestigial phases, and demonstrate how this leads to intertwined spin-orbital coupled orders. The electronic orders induced in this manner include the well-known ferro-orbital order arising in the nematic case, but also a more exotic spin-current order. We show how a number of these induced electronic orders lead to the lifting of the spin-degeneracy of the bands. The vestigial phases exhibit unique features when subjected to external electromagnetic fields. These are discussed in Sec. IV. In Sec. V we discuss how our approach changes depending on the stacking of the FeAs/Se layers, contrasting

1111, 111, 11 compounds and 122 compounds. Finally, conclusions are presented in Sec. VI. Additionally, we include two appendices containing technical details of the Hamiltonian used (Appendix A) and the derivation of the fermionic bilinears (Appendix B).

II. COMPOSITE SPIN ORDER IN THE VESTIGIAL PHASES

A. Magnetically ordered states

Recent experiments unveiled an unexpected complexity of the phase diagram of underdoped iron-based superconductors, which rivals that of underdoped cuprates. Our goal is to formulate a unifying framework in which the observed magnetic and non-magnetic orders arise from the same basic interactions, thus providing an organizing principle to describe and predict the behavior of underdoped iron-based superconductors without resorting to fine-tuned multi-critical points. The main idea is that all these phases can be described as condensations of simple or composite combinations of the components of the six-dimensional super-vector:

$$\boldsymbol{\mathcal{M}} = \left(\begin{array}{cccccc} M_{1,x} & M_{1,y} & M_{1,z} & M_{2,x} & M_{2,y} & M_{2,z} \end{array} \right) . \quad (3)$$

Here, $M_{a,\mu}$ are the components of the staggered magnetizatons $\mathbf{M}_1$ and $\mathbf{M}_2$ given in Eq. (1). In this framework, the primary degrees of freedom are the magnetic ones. This does not mean that orbital degrees of freedom are irrelevant – much to the contrary, they are essential to correctly describe the vestigial phases, as shown in Ref. 23. Empirically, it is well established that most iron superconductors display sharp magnetic fluctuations around the wave-vectors $\mathbf{Q}_1 = (\pi, 0)$ and $\mathbf{Q}_2 = (0, \pi)$ [50]. Microscopically, one expects on general grounds that repulsive electronic interactions are responsible for the enhancement of these fluctuations [46]. In this paper, we will not discuss the microscopic origin of this magnetism. Instead, we simply note that both weak-coupling [20, 38, 44–46, 51] and strong-coupling [52–55] approaches give magnetic fluctuations peaked at these ordering vectors [56].

In the absence of a lattice, the elements of $\boldsymbol{\mathcal{M}}$ would transform as an irreducible representation (irrep) of the $SO(6)$ group. There is a huge degeneracy of magnetic ground states that give the same amplitude of the super-vector $\boldsymbol{\mathcal{M}}$. The vast majority of these states are not realized in the iron-based superconductors. This reflects the important fact that this enlarged $SO(6)$ symmetry is merely a theoretical construct, as the existence of the lattice immediately constrains the possible combinations of the elements of $\boldsymbol{\mathcal{M}}$ to those that obey the crystal lattice symmetries. We stress that the magnetic order parameters are not SO(6) invariant. Below we use group theory to show how the crystal lattice restricts the symmetry of the magnetic order parameters.

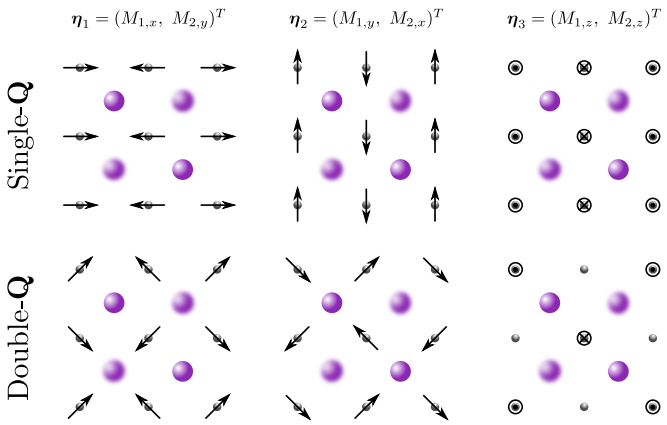

Figure 3. Illustration of the possible magnetic orders for each order parameter $\boldsymbol{\eta}_i$, with transforms as a two-dimensional irreducible representation of the space group. The double-$\mathbf{Q}$ structures for $\boldsymbol{\eta}_1$ and $\boldsymbol{\eta}_2$ are the in-plane hedgehog- and loop-SVC phases, respectively. For $\boldsymbol{\eta}_3$, the double-$\mathbf{Q}$ phase is denoted the charge-spin density-wave phase. All single-$\mathbf{Q}$ phases are stripe magnetically ordered states.

In the simple approximation where the As/Se atoms are neglected, and the crystal is described as a single-Fe square lattice, the six components of $\boldsymbol{\mathcal{M}}$ do not transform according to an irreducible representation of the $SO(6)$ group, but instead according to an irrep of the $C_{4v}''' \otimes SO(3)$ group, as discussed in Ref. 7. Here, C_{4v}''' is the extended point group corresponding to the point group C_{4v} supplemented by three translations along $\hat{\mathbf{x}}$, $\hat{\mathbf{y}}$, and $\hat{\mathbf{x}} + \hat{\mathbf{y}}$. The translations are necessary because the order parameters $M_{a,\mu}$ break the translational symmetry of the lattice. Note that, for our purposes, we neglected the inversion symmetry and considered C_{4v} instead of D_{4h}. As discussed in Ref. 7, the six elements of $\boldsymbol{\mathcal{M}}$ transform as the product of irreps $E_5 \otimes \Gamma^{S=1}$, where E_5 is a two-dimensional irreducible representation of C_{4v}''' and $\Gamma^{S=1}$ is the standard 3-dimensional irreducible representation of $SO(3)$. This warrants writing $\boldsymbol{\mathcal{M}} = (\mathbf{M}_1, \mathbf{M}_2)^T$ and identifying the appropriate order parameters as the three-dimensional vectors $\mathbf{M}_1$ and $\mathbf{M}_2$, instead of $\boldsymbol{\mathcal{M}}$. The resulting free energy, which can be constructed by imposing that its elements transform trivially under the group symmetry operations, becomes:

$$\begin{aligned} F[\mathbf{M}_a] = & \frac{a}{2}\left(M_1^2 + M_2^2\right) + \frac{u}{4}\left(M_1^2 + M_2^2\right)^2 \\ & - \frac{g}{4}\left(M_1^2 - M_2^2\right)^2 + w\left(\mathbf{M}_1 \cdot \mathbf{M}_2\right)^2 . \end{aligned} \quad (4)$$

Clearly, while the first two terms only depend on the amplitude of the super-vector $\boldsymbol{\mathcal{M}}$, the last two terms explicitly break $SO(6)$ symmetry. This free-energy expansion, and the field theory resulting from it, have been widely studied in several papers in the context of the pnictides [20, 23, 38, 39, 42, 43, 45, 57]. We just quote here the result that there are only three possible ground states, which are determined by the quartic coefficients g and w: the single-$\mathbf{Q}$ stripe magnetic state, where $\mathbf{M}_1 \neq 0$ and

$\mathbf{M}_2 = 0$ (or vice-versa); the non-collinear double-$\mathbf{Q}$ spin-vortex crystal state, where $M_1 = M_2$ and $\mathbf{M}_1 \perp \mathbf{M}_2$; and the collinear double-$\mathbf{Q}$ charge-spin density-wave, where $M_1 = M_2$ and $\mathbf{M}_1 \parallel \mathbf{M}_2$. All these states have been observed in the iron-based superconductors [29, 33, 58–60].

Although the magnetic properties of these systems are decently described within the approximation of a single-Fe square lattice, the symmetries of the actual FeAs/Se layer are different than those of the simple square lattice. Most notably, there is a glide plane symmetry originating from the puckering of the As/Se atoms above and below the Fe plane. The immediate consequence of including the As/Se atoms is that the unit cell doubles and rotates by 45° (see Fig. 2). Note that this unit cell is invariant under a four-fold rotation only if it is accompanied by a mirror reflection. There are also important consequences for the electronic structure, as the different Fe $3d$ orbitals do not necessarily transform the same way under the glide plane symmetry operation [61, 62]. Crucially, a sizable atomic spin-orbit coupling $\lambda \mathbf{S} \cdot \mathbf{L}$ is observed in these materials ($\lambda \sim 20$ meV [48]). As a result, the spin-space $SO(3)$ symmetry is broken, and the six magnetic components no longer transform according to an irrep of the $C_{4v}^{'''} \otimes SO(3)$ group. Instead, the relevant group is the space-group of a single FeAs/Se layer, which is the non-symmorphic $P4/nmm$ group (group number 129) [17, 40].

In this case, the six elements of $\boldsymbol{\mathcal{M}}$ cannot be organized in the two three-dimensional vectors $\mathbf{M}_1$ and $\mathbf{M}_2$. Due to the doubling and 45° rotation of the Fe-square unit cell, the two wave-vectors $\mathbf{Q}_1 = (\pi, 0)$ and $\mathbf{Q}_2 = (0, \pi)$ are folded onto the same wave-vector $\mathbf{Q}_M = (\pi, \pi)$ (see Fig. 2). As a result, the six elements of $\boldsymbol{\mathcal{M}}$ must transform according to different irreps of the space group $P4/nmm$ at the $M \equiv (\pi, \pi)$ point of the crystallographic Brillouin zone. It was shown in Ref. 40 that all irreps of $P4/nmm$ at M are two-dimensional. As a result, the six elements of $\boldsymbol{\mathcal{M}}$ should be organized in terms of three different two-dimensional irreps, denoted by E_{M1}, E_{M2}, and E_{M3} (using the terminology of Ref. 40). The corresponding two-dimensional order parameters are, respectively, the $\boldsymbol{\eta}_1$, $\boldsymbol{\eta}_2$, and $\boldsymbol{\eta}_3$ vectors given by Eq. (2). Their physical meaning can be understood in a straightforward way: in the presence of spin-orbit coupling, $M_{1,x}$, $M_{1,y}$, and $M_{1,z}$ become independent. Each of these order parameters have a partner related by a simultaneous 90° rotation around $\hat{\mathbf{z}}$ in both real and spin spaces, corresponding to $M_{2,y}$, $M_{2,x}$, and $M_{2,z}$.

The field theory for the magnetic degrees of freedom should thus be expressed in terms of the two-component vectors $\boldsymbol{\eta}_\alpha$, rather than the three-component vectors $\mathbf{M}_a$. Imposing that the free-energy expansion transforms trivially under the operations of the space group $P4/nmm$, we find:

$$F[\boldsymbol{\eta}_\alpha] = \sum_\alpha \frac{a_\alpha}{2} \left(\boldsymbol{\eta}_\alpha \tau^0 \boldsymbol{\eta}_\alpha\right) + \sum_{\alpha,\beta} \frac{u_{\alpha\beta}}{4} \left(\boldsymbol{\eta}_\alpha \tau^0 \boldsymbol{\eta}_\beta\right)^2 - \sum_{\alpha,\beta} \frac{g_{\alpha\beta}}{4} \left(\boldsymbol{\eta}_\alpha \tau^z \boldsymbol{\eta}_\beta\right)^2 + \sum_{\alpha \neq \beta} \frac{w_{\alpha\beta}}{4} \left(\boldsymbol{\eta}_\alpha \tau^x \boldsymbol{\eta}_\beta\right)^2 . \quad (5)$$

Here, $\alpha, \beta = 1, 2, 3$ and τ^j are Pauli matrices that live in the two-dimensional "internal" space of $\boldsymbol{\eta}_\alpha$. Symmetry constrains a number of the coefficients, e.g. $u_{13} + g_{13} = -w_{13}$ and $u_{23} + g_{23} = -w_{23}$. Note that the quadratic term was previously obtained in Refs. 41 and 63. Moreover, the $w_{\alpha\beta}$-coefficients play no role at the magnetic transition [64, 65]. We emphasize that several of the magnetic properties derived from Eq. (4) still hold in this alternative formulation. But as we show below, the field theory that respects the actual crystallographic symmetries of the FeAs/Se layers provides unique insights into the rich interplay between spin and orbital degrees of freedom.

The six different ground states of Eq. (5) are obtained by direct minimization (see also Ref. 41), and are shown in Fig. 3. For each of the three irreps, represented by $\boldsymbol{\eta}_\alpha$, there are two possible magnetic ground states, corresponding to single-$\mathbf{Q}$ configurations (i.e. condensation of one of the components of $\boldsymbol{\eta}_\alpha$) or double-$\mathbf{Q}$ configurations (i.e. simultaneous condensation of both components of $\boldsymbol{\eta}_\alpha$). Specifically, the ground states associated with $\boldsymbol{\eta}_1$ are the single-$\mathbf{Q}$ stripe magnetic phase with moments pointing parallel to the wave-vectors $\mathbf{Q}_1 = (\pi, 0)$ and $\mathbf{Q}_2 = (0, \pi)$, and the double-$\mathbf{Q}$ hedgehog spin-vortex crystal phase [33]. Similarly, the ground states associated with $\boldsymbol{\eta}_2$ are the single-$\mathbf{Q}$ stripe magnetic phase with moments pointing in-plane, but perpendicular to the wave-vectors $\mathbf{Q}_1 = (\pi, 0)$ and $\mathbf{Q}_2 = (0, \pi)$, and the double-$\mathbf{Q}$ loop spin-vortex crystal phase. Finally, the ground states associated with $\boldsymbol{\eta}_3$ are the single-$\mathbf{Q}$ stripe magnetic phase with moments pointing out-of-plane, and the double-$\mathbf{Q}$ charge-spin density-wave [29]. Note that these six states are a subset of the states obtained from the minimization of Eq. (4). The restrictions arise from the symmetry properties that the spin components must obey due to the finite spin-orbit coupling.

B. Vestigial orders

The vestigial orders in terms of the $\mathbf{M}_a$ order parameters were previously discussed elsewhere by one of us [47]. Here, we use group-theory to systematically derive all vestigial orders in terms of the $\boldsymbol{\eta}_\alpha$ order parameters. This corresponds to much more than a simple change of basis, as only the $\boldsymbol{\eta}_\alpha$ vectors transform according to the actual crystallographic space group. This will give rise to important qualitative differences between the two cases. For instance, while certain vestigial phases described by the free energy in Eq. (4) break translational symmetry

and are associated with continuous order parameters, all vestigial phases described by Eq. (5) preserve translational symmetry and are associated with discrete order parameters.

A vestigial order parameter is a composite order parameter that can order even in the absence of the primary order, and that breaks a subset of the symmetries broken by the primary order parameter (for a review, see Ref. 7). Vestigial order can only appear if the primary order parameter transforms as a multi-dimensional irrep, i.e. if the group is non-Abelian. In our case, we thus search for bilinear combinations φ^j_α of the primary order parameters $\boldsymbol{\eta}_\alpha$ that do not transform trivially under the operations of the space group $P4/nmm$:

$$\varphi^j_\alpha = \sum_{\mu,\nu} \eta^\mu_\alpha \Lambda^j_{\mu\nu} \eta^\nu_\alpha \,. \tag{6}$$

Here, $\mu, \nu = 1, 2$ denote the two components of the vector $\boldsymbol{\eta}_\alpha$ and $\Lambda^j_{\mu\nu}$ is a 2×2 matrix. Since the three $\boldsymbol{\eta}_\alpha$ belong to different irreps, and long-range magnetic order develops only within a single irrep channel, we consider only the composite order parameters associated with each irrep separately. This is in agreement with previous RG calculations of Eq. (4) in the presence of spin-orbit coupling [64, 65].

The 2×2 matrices $\Lambda^j_{\mu\nu}$ can be generally expressed in terms of Pauli matrices $\boldsymbol{\tau}$. Their explicit expressions are obtained by the decomposition of the products of irreps E_{Mi} [40]:

$$E_{M1(M2)} \otimes E_{M1(M2)} = A_{1g} \oplus B_{2g} \oplus A_{2u} \oplus B_{1u} \tag{7}$$
$$E_{M3} \otimes E_{M3} = A_{1g} \oplus B_{2g} \oplus A_{1u} \oplus B_{2u} \,. \tag{8}$$

The fact that both inversion-even (g) and inversion-odd (u) one-dimensional irreps appear is because the two components of the two-dimensional irreps transform oppositely under the glide-plane symmetry. Note that, because $2\mathbf{Q}_M = (2\pi, 2\pi)$, the irreps on the right-hand side are those of the $P4/nmm$ space group at the $\Gamma \equiv (0, 0)$ point of the crystallographic Brillouin zone, which is equivalent to the familiar point group D_{4h}. Among those, it is not possible to form non-zero bilinears involving $\boldsymbol{\eta}_\alpha$ that transform as B_{1u} and A_{1u}. Consequently, for each α, there are only two possible composite order parameters that transform non-trivially under D_{4h} (i.e. that do not transform as A_{1g}), namely:

$$\begin{aligned} \varphi^z_\alpha &\equiv \boldsymbol{\eta}_\alpha \tau^z \boldsymbol{\eta}_\alpha \,, \\ \varphi^x_\alpha &\equiv \boldsymbol{\eta}_\alpha \tau^x \boldsymbol{\eta}_\alpha \,. \end{aligned} \tag{9}$$

In terms of the original order parameters $\mathbf{M}_a$, we have:

$$\begin{aligned} \varphi^z_1 &= M^2_{1,x} - M^2_{2,y} \,, \quad \varphi^x_1 = 2M_{1,x}M_{2,y} \,, \\ \varphi^z_2 &= M^2_{1,y} - M^2_{2,x} \,, \quad \varphi^x_2 = 2M_{1,y}M_{2,x} \,, \\ \varphi^z_3 &= M^2_{1,z} - M^2_{2,z} \,, \quad \varphi^x_3 = 2M_{1,z}M_{2,z} \,. \end{aligned} \tag{10}$$

All these composite order parameters have zero wavevector, and thus correspond to intra-unit cell order. In particular, φ^z_1, φ^z_2, and φ^z_3 transform as the B_{2g} irrep of D_{4h}; φ^x_1 and φ^x_2 transform as A_{2u}; and φ^x_3 transform as B_{2u}. Because order parameters that break the same symmetry must necessarily couple bilinearly in the free energy expansion, they must either be all zero or all non-zero at the same time. Therefore, we identify three distinct vestigial phases, represented by the order parameters: $\Phi_{B_{2g}} \propto \varphi^z_1 \propto \varphi^z_3 \propto \varphi^z_2$; $\Phi_{A_{2u}} \propto \varphi^x_1 \propto \varphi^x_2$; $\Phi_{B_{2u}} \propto \varphi^x_3$. All of them are Ising-like, zero wave-vector order parameters; the subscript just indicates how they transform under the D_{4h} group. In the next section, we will see that they correspond to nematic order, spin-current order, and checkerboard charge order, respectively. Interestingly, the existence of three inter-related spin-driven Ising-nematic order parameters, φ^z_1, φ^z_2, and φ^z_2 have been recently reported in an NMR study of a detwinned 122 iron pnictide [66].

Having established the vestigial order parameters, we now discuss the actual vestigial phases. Formally, a vestigial phase is that in which the symmetry-breaking composite order parameter is non-zero, but the primary order parameter vanishes:

$$\left\langle \boldsymbol{\eta}_\alpha \tau^{(x,z)} \boldsymbol{\eta}_\alpha \right\rangle \neq 0 \,, \quad \langle \boldsymbol{\eta}_\alpha \rangle = 0 \,. \tag{11}$$

Clearly, if $\langle \boldsymbol{\eta}_\alpha \rangle \neq 0$, it follows necessarily that at least one of the composite orders is non-zero, $\left\langle \boldsymbol{\eta}_\alpha \tau^{(x,z)} \boldsymbol{\eta}_\alpha \right\rangle \neq 0$. The non-trivial aspect of the condition above arises from the fact that the composite order can be finite even if the primary order is not. Note also that $\langle \boldsymbol{\eta}_\alpha \boldsymbol{\tau}^y \boldsymbol{\eta}_\alpha \rangle$ is identically zero, as τ^y is antisymmetric, and that the non-symmetry breaking composite combination $\left\langle \boldsymbol{\eta}_\alpha \tau^0 \boldsymbol{\eta}_\alpha \right\rangle$ is always non-zero, as it transforms as the trivial A_{1g} irrep of D_{4h}. Physically, the latter corresponds simply to magnetic amplitude fluctuations. To determine whether and when condition (11) is satisfied, phenomenological considerations are not enough, and one must resort to microscopic calculations, which will depend on the model. Importantly, in our case, both the vestigial and primary magnetic order parameters are Ising-like. Generally, it is possible that the two Ising transitions are split and second- or first-order (in which case there is a regime of vestigial phase) or simultaneous and first-order (in which case there is no vestigial phase). Both regimes have been theoretically seen, depending on model parameters [20, 21].

The outcome of our analysis is shown in Fig. 1. It is remarkable that all these different broken-symmetry states arise from the same primary degrees of freedom, which ultimately go back to the six-dimensional supervector $\boldsymbol{\mathcal{M}}$ in Eq. (3). We emphasize that each of the three classes of magnetic order, represented by the irrep E_{Mi} and shown in Fig. 3, support two possible types of vestigial order parameters: $\boldsymbol{\eta}_\alpha \tau^z \boldsymbol{\eta}_\alpha$, associated with the single-$\mathbf{Q}$ phase, and $\boldsymbol{\eta}_\alpha \tau^x \boldsymbol{\eta}_\alpha$, associated with the double-$\mathbf{Q}$ phase. While all three classes support a B_{2g} nematic vestigial phase, only the $E_{M1,M2}$ classes support an A_{2u} spin-current vestigial states, whereas only E_{M3} supports a B_{2u} charge-order vestigial phase.

III. ORBITAL-ORDER PATTERNS IN THE VESTIGIAL PHASES

Our analysis so far has focused exclusively on the spin degrees of freedom. However, orbital degrees of freedom are essential to describe the properties of the vestigial phases, particularly since it is the very existence of a spin-orbit coupling that changes the form of the magnetic free-energy from Eq. (4) to Eq. (5).

To proceed, we must first define what we mean by orbital degrees of freedom, since the five $3d$ Fe orbitals are generally hybridized throughout the Brillouin zone, and are thus not generically good quantum numbers. However, if we focus on the low-energy states near the Fermi level, we can restrict our analysis to the orbitals that give the dominant spectral weight, namely, the d_{xz}, d_{yz}, and d_{xy} orbitals. Moreover, because the Fermi pockets are typically small, we can focus on the states close to the high-symmetry points of the crystallographic Brillouin zone, i.e. the $\Gamma = (0,0)$ and $M = (\pi,\pi)$ points. Fortunately, at these high-symmetry points, we can define pure orbital states. Thus, we can label the Bloch states near the Fermi level by their orbital content, following the procedure outlined in Ref. 40. Near the Γ point, the Fermi surface consists of two small hole pockets, and the relevant orbitals are the d_{xz} and d_{yz}, which transform as the E_g representation of the D_{4h} group. Thus, we define the electronic doublet:

$$\Psi_{\Gamma,s}(\mathbf{K}) = \begin{pmatrix} d_{yz,s}(\mathbf{k}) \\ -d_{xz,s}(\mathbf{k}) \end{pmatrix} , \tag{12}$$

in terms of the xz and yz orbital operators. Here, s denotes the spin quantum number. We use $\mathbf{K}/\mathbf{X}$ to denote a momentum in the crystallographic Brillouin zone/unit cell, while $\mathbf{k}/\mathbf{x}$ corresponds to the 1-Fe Brillouin zone/unit cell (see Fig. 2). Near the M point, there are two small electron pockets whose orbital contents are d_{xz}/d_{yz} and d_{xy}. Because all irreps of $P4/nmm$ at M are doubly degenerate, we define two electronic doublets:

$$\begin{aligned} \Psi_{M_+,s}(\mathbf{K}+\mathbf{Q}_M) &= \begin{pmatrix} d_{xz,s}(\mathbf{k}+\mathbf{Q}_2) \\ d_{xy,s}(\mathbf{k}+\mathbf{Q}_1) \end{pmatrix} , \\ \Psi_{M_-,s}(\mathbf{K}+\mathbf{Q}_M) &= \begin{pmatrix} d_{yz,s}(\mathbf{k}+\mathbf{Q}_1) \\ d_{xy,s}(\mathbf{k}+\mathbf{Q}_2) \end{pmatrix} . \end{aligned} \tag{13}$$

While the two elements of $\Psi_{M_+,\sigma}$ transform as the "upper" elements of the E_{M1} and E_{M3} irreducible representations, the two elements of $\Psi_{M_-,\sigma}$ transform as the "lower" elements of E_{M1} and E_{M3} [40]. The generic non-interacting Hamiltonian in terms of these three doublet operators was discussed in Ref. 40, and is shown again in Appendix A. Because its form is enforced only by the symmetries of the $P4/nmm$ group, it can be used to fit any experimentally determined band dispersion. Note that while the Bloch states Ψ_Γ, $\Psi_{M_\pm}$ are defined in the crystallographic Brillouin zone, the orbital operators d_{xz}, d_{yz}, d_{xy} are defined in the 1-Fe Brillouin zone.

To obtain the orbital order patterns of each of the vestigial phases, all we need now is to find the fermionic bilinears $\left\langle \Psi_a^\dagger \hat{\Lambda} \Psi_b \right\rangle$, where $\hat{\Lambda}$ is a vertex in the space of electronic operators, that transform according to the B_{2g}, A_{2u}, and B_{2u} irreps of the D_{4h} group. Since the vestigial orders have zero wave-vector, we look for combinations $\left\langle \Psi_\Gamma^\dagger \hat{\Lambda} \Psi_\Gamma \right\rangle$ and $\left\langle \Psi_{M_\pm}^\dagger \hat{\Lambda} \Psi_{M_\pm} \right\rangle$. Using the product tables for the $P4/nmm$ group and including the role of the spin operators, we obtain the orbital order parameters detailed below. For the full derivation, see Appendix B.

A. B_{2g} nematic order

We start with the case of the $\Phi_{B_{2g}}$ vestigial order, which is the vestigial phase associated with the E_{M_1}, E_{M_2}, and E_{M_3} single-$\mathbf{Q}$ stripe magnetic phase, as discussed in Sec. II. There are three different types of orbital order parameters that appear concomitantly with the condensation of $\Phi_{B_{2g}}$ (see Ref. 67):

$$\Delta^{(1)}_{B_{2g}} = \left\langle d^\dagger_{yz,s}(\mathbf{k}) d_{yz,s}(\mathbf{k}) - d^\dagger_{xz,s}(\mathbf{k}) d_{xz,s}(\mathbf{k}) \right\rangle \tag{14}$$

$$\begin{aligned} \Delta^{(2)}_{B_{2g}} = \big\langle & d^\dagger_{yz,s}(\mathbf{k}+\mathbf{Q}_1) d_{yz,s}(\mathbf{k}+\mathbf{Q}_1) \\ & - d^\dagger_{xz,s}(\mathbf{k}+\mathbf{Q}_2) d_{xz,s}(\mathbf{k}+\mathbf{Q}_2) \big\rangle \end{aligned} \tag{15}$$

$$\begin{aligned} \Delta^{(3)}_{B_{2g}} = \big\langle & d^\dagger_{xy,s}(\mathbf{k}+\mathbf{Q}_1) d_{xy,s}(\mathbf{k}+\mathbf{Q}_1) \\ & - d^\dagger_{xy,s}(\mathbf{k}+\mathbf{Q}_2) d_{xy,s}(\mathbf{k}+\mathbf{Q}_2) \big\rangle . \end{aligned} \tag{16}$$

Note that we have omitted the momentum summations for convenience. The first two terms can be expressed as combinations of onsite ferro-orbital order and bond-orbital order involving the d_{xz} and d_{yz} orbitals, whereas the third term corresponds to bond orbital order involving the d_{xy} orbital. The breaking of tetragonal symmetry warrants identifying this vestigial phase as a nematic phase. We emphasize that this orbital pattern is rather different than a uniform occupation of the d_{xz} and d_{yz} orbitals, as it has previously been pointed out theoretically in [68–70] and observed experimentally in Refs. 71 and 72.

The real-space orbital order patterns are illustrated in Figs. 4(a) and (b). While the former represents an onsite d_{xz}/d_{yz} ferro-orbital order, the latter represents a hopping anisotropy between nearest-neighbors d_{xy} orbitals (i.e. bond order). In Figs. 4(c) and (d), we show the impact of these orbital order parameters on the band dispersions and on the Fermi surface. The main effects are the well-known splitting of the energy doublets at the M point and the Pomeranchuk-like distortion of the Fermi pockets, which are no longer C_4 symmetric. In these figures, we also included the finite atomic spin-orbit coupling, which lifts the degeneracy of the energy doublet at Γ and hybridizes the two electron pockets already in the non-nematic phase [48, 67].

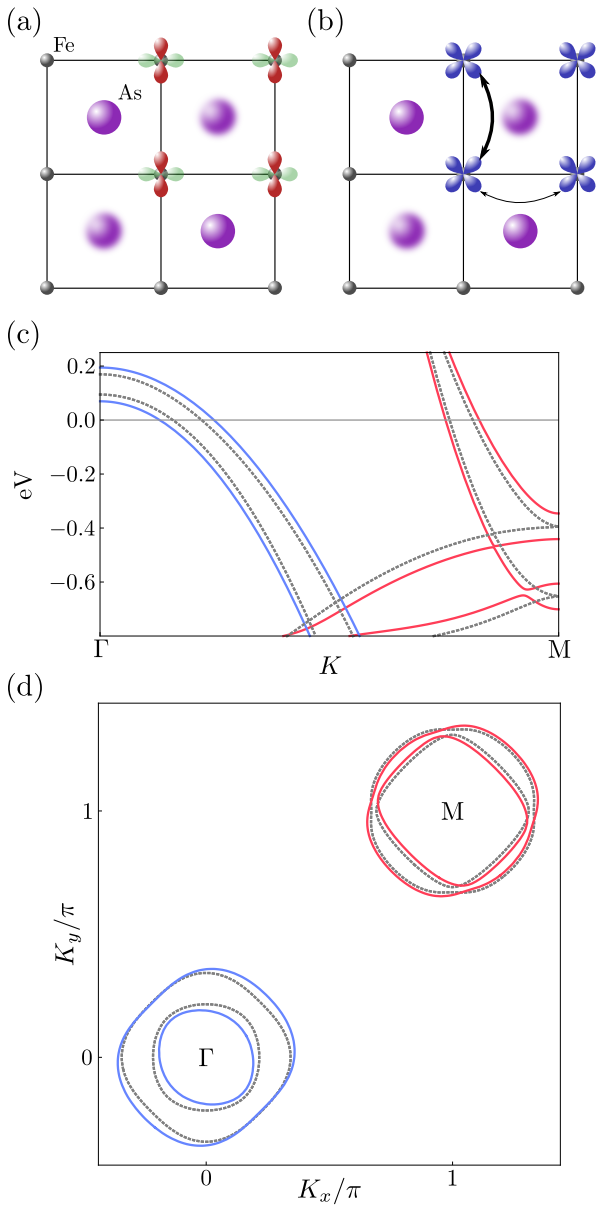

Figure 4. Effects of B_{2g} vestigial nematic order. In (a) we illustrate the ferro-orbital order involving the d_{xz} and d_{yz} Fe $3d$-orbitals ($\Delta^{(1)}_{B_{2g}} \neq 0$) while in (b), the bond-nematic order (hopping anisotropy) involving the d_{xy} orbitals ($\Delta^{(3)}_{B_{2g}} \neq 0$). The band structure and Fermi surface in the vestigial phase are shown in (c) and (d), respectively. The dotted lines show the band structure in the non-ordered phase. Note the Pomeranchuk-type distortion of the Fermi surface. The parameters used here are given in Appendix A.

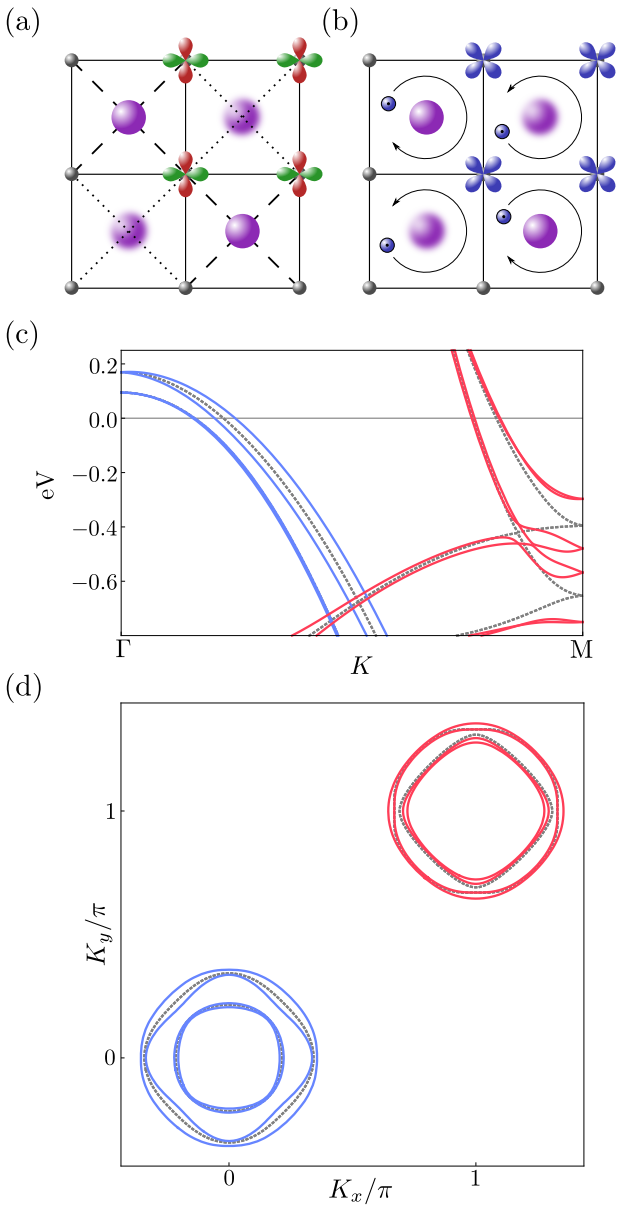

Figure 5. Effects of A_{2u} vestigial spin-current order. In (a), the bonds between next-nearest-neighbor Fe-atoms become inequivalent in a staggered pattern as a result of $\Delta^{(1)}_{A_{2u}} \neq 0$. This renders the As/Se atoms above and below the Fe-plane inequivalent as well. In (b), we illustrate the formation of staggered spin-currents involving the d_{xy} orbitals ($\Delta^{(2)}_{A_{2u}} \neq 0$). The band structure and Fermi surface in the vestigial phase are shown in (c) and (d), respectively. Note the doubling of the number of bands due to the lifting of spin degeneracy. The parameters used here are given in Appendix A.

B. A_{2u} spin-current order

Let us now consider the vestigial phase with $\Phi_{A_{2u}}$ order parameter, which is associated with the E_{M_1}, E_{M_2} double-**Q** spin-vortex crystal phase discussed in Sec. II. There are two momentum-independent fermionic bilinears that transform as A_{2u}; both involve only states at

the M point:

$$\Delta^{(1)}_{A_{2u}} = \left\langle d^\dagger_{xz,s}(\mathbf{k}+\mathbf{Q}_2) d_{yz,s}(\mathbf{k}+\mathbf{Q}_1) + \text{h.c.} \right\rangle \tag{17}$$

$$\Delta^{(2)}_{A_{2u}} = i \left\langle d^\dagger_{xy,s}(\mathbf{k}+\mathbf{Q}_2) \sigma^z_{ss'} d_{xy,s'}(\mathbf{k}+\mathbf{Q}_1) - \text{h.c.} \right\rangle . \tag{18}$$

The first term corresponds to an intra-unit cell staggered deformation of the bonds connecting next-nearest-neighbor Fe atoms, and as such renders the positions of the As/Se atoms above and below the Fe plane inequivalent [73]. The second term corresponds to an intra-unit cell staggered spin-current, polarized along the z axis, involving only the d_{xy} orbitals – hence the identification of this phase as spin-current order. Both types of order are illustrated, in real space, in Figs. 5(a) and (b), respectively. Additional spin-dependent terms are discussed in Appendix B.

Although, at first sight, it may seem that the states near Γ are not affected by $\Phi_{A_{2u}}$, this only happens if we restrict the analysis to momentum-independent fermionic bilinears. Allowing for terms that are linear in momentum, we find several orbital-order combinations that are reminiscent of the Rashba- and Dresselhaus-type terms typically found in systems that break inversion symmetry. For instance, two of these terms are:

$$\Delta^{(3)}_{A_{2u}} = \langle (k_x \sigma^y_{ss'} - k_y \sigma^x_{ss'}) \left(d^\dagger_{xz,s}(\mathbf{k}) d_{xz,s'}(\mathbf{k}) + d^\dagger_{yz,s}(\mathbf{k}) d_{yz,s'}(\mathbf{k}) \right) \rangle \tag{19}$$

$$\Delta^{(5)}_{A_{2u}} = \langle (k_x \sigma^x_{ss'} - k_y \sigma^y_{ss'}) \left(d^\dagger_{xz,s}(\mathbf{k}) d_{yz,s'}(\mathbf{k}) + d^\dagger_{yz,s}(\mathbf{k}) d_{xz,s'}(\mathbf{k}) \right) \rangle . \tag{20}$$

Recall that k_x and k_y refer to momenta in the 1-Fe Brillouin zone and σ^x and σ^y refer to spins along the Fe-Fe bonds. All four allowed linear-in-momentum terms are shown explicitly in Appendix B.

In Figs. 5(c) and (d), we show the electronic band dispersion reconstructed by all these orbital-order patterns. Besides the splitting of the energy doublets at M, which is similar to the case of the nematic vestigial order, the most salient feature is the doubling of the number of bands, despite the absence of translational or rotational symmetry breaking. This doubling is a consequence of the fact that the bands are no longer spin-degenerate due to the combination of a finite spin-orbit coupling and an order parameter that breaks inversion symmetry (i.e. it transforms as A_{2u}). Indeed, such a band splitting is commonly found in systems where the explicit breaking of inversion symmetry (e.g. by an applied electric field) induces a Rashba coupling. What is unique to the A_{2u} vestigial phase is that the Rashba-type coupling is the result of an spontaneous symmetry-breaking. Being a composite spin order parameter, its magnitude is set by the strength of magnetic fluctuations, which could in principle be sizable near a magnetic critical point. It is important to emphasize that the Fermi surface remains symmetric under a 90° rotation and under an in-plane inversion. This is a consequence of the fact that the vestigial order parameter transforms as A_{2u}.

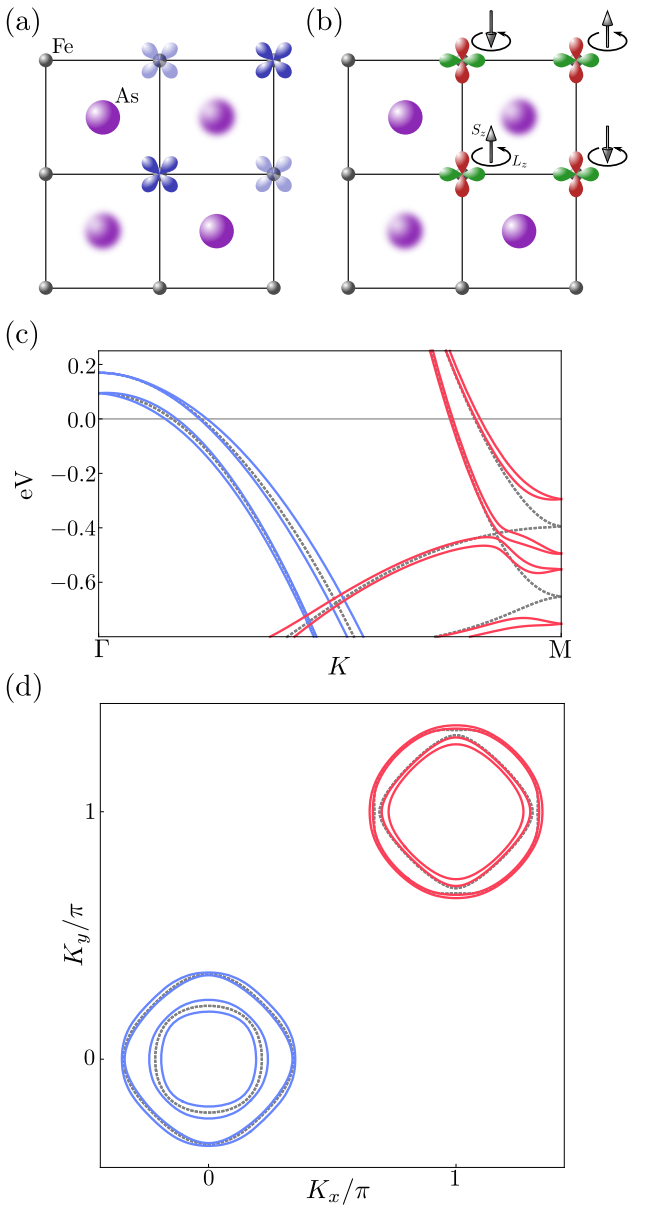

Figure 6. Effects of the B_{2u} vestigial charge order. In (a) we show the induced charge order in the d_{xy} orbital ($\Delta^{(1)}_{B_{2u}} \neq 0$) and in (b) the emergence of a staggered $L_z S_z$ spin-orbital coupling between the d_{xz} and d_{yz} orbitals ($\Delta^{(2)}_{B_{2u}} \neq 0$). The band structure and Fermi surfaces in the vestigial phase are shown in (c) and (d), respectively. Note the doubling of the number of bands due to the lifting of spin degeneracy. The parameters used here are given in Appendix A.

C. B_{2u} charge order

Finally, we analyze the orbital order patterns associated with the vestigial order with $\Phi_{B_{2u}}$ order parameter, which is related to the E_{M_3} double-$\mathbf{Q}$ charge-spin density-wave phase. There are two momentum-

independent fermionic bilinears transforming as B_{2u}:

$$\Delta^{(1)}_{B_{2u}} = \left\langle d^\dagger_{xy,s}(\mathbf{k}+\mathbf{Q}_2) d_{xy,s}(\mathbf{k}+\mathbf{Q}_1) + \text{h.c.} \right\rangle \tag{21}$$

$$\Delta^{(2)}_{B_{2u}} = i \left\langle d^\dagger_{xz,s}(\mathbf{k}+\mathbf{Q}_2) \sigma^z_{ss'} d_{yz,s'}(\mathbf{k}+\mathbf{Q}_1) - \text{h.c.} \right\rangle . \tag{22}$$

The first term corresponds to an occupation imbalance of the d_{xy} orbital on neighboring sites, as illustrated in Fig. 6(a). Note that this is an intra-unit cell order. The second term corresponds to an intra-unit cell staggered $L_z S_z$-type spin-orbit coupling, illustrated in Fig. 6(b). Appendix B shows additional spin-dependent terms are discussed.

As with the case of A_{2u} vestigial order, electronic states near the Γ point are affected by terms linear in momentum. As explained above, these terms resemble the Rashba- and Dresselhaus-type spin-orbit couplings commonly found in systems that break inversion symmetry. In our case however, the multi-orbital structure allows for multiple inequivalent terms:

$$\Delta^{(3)}_{B_{2u}} = \langle (k_x \sigma^x_{ss'} - k_y \sigma^y_{ss'}) \left(d^\dagger_{xz,s}(\mathbf{k}) d_{xz,s'}(\mathbf{k}) + d^\dagger_{yz,s}(\mathbf{k}) d_{yz,s'}(\mathbf{k}) \right) \rangle \tag{23}$$

$$\Delta^{(5)}_{B_{2u}} = \langle (k_x \sigma^y_{ss'} - k_y \sigma^x_{ss'}) \left(d^\dagger_{xz,s}(\mathbf{k}) d_{yz,s'}(\mathbf{k}) + d^\dagger_{yz,s}(\mathbf{k}) d_{xz,s'}(\mathbf{k}) \right) \rangle . \tag{24}$$

All the induced spin-orbit terms are listed in Appendix B. The reconstruction of the electronic dispersion in the vestigial phase that displays B_{2u} order is shown in Figs. 6(c) and (d). As with the $\Phi_{A_{2u}}$ case, the spin-degeneracy of the bands is lifted and translational symmetry remains unbroken. The doublets at M are split in a manner reminiscent of the B_{2g} nematic case, although the Fermi surface remains symmetric under a 90° rotation since the order parameter transforms as B_{2u}.

IV. EXPERIMENTAL CONSEQUENCES

The symmetry classification above reveals the existence of three different types of vestigial phases associated with the magnetic ground states of the iron pnictides, which trigger unique orbital order patterns. All these vestigial order parameters are Ising-like (i.e. scalar) that have zero in-plane wave-vector. As such, they transform as different irreducible representations of the $P4/nmm$ group at the Γ point, which coincide with the irreps of the D_{4h} space group. In particular, we found a vestigial nematic B_{2g} phase, a vestigial spin-current A_{2u} phase, and a vestigial charge-ordered B_{2u} phase. In this section, we discuss different experimental manifestations of these vestigial orders based on their coupling to non-electronic degrees of freedom, such as the lattice, as well as to external electromagnetic fields.

A. Coupling to the lattice

In the long wavelength limit, the elastic degrees of freedom are described in terms of derivatives of the displacement vector $\mathbf{U}$. For a tetragonal lattice, there are six independent strain modes. Two of them transform as A_{1g} and do not change the symmetry of the lattice (e.g. volume collapse); two of them involve out-of-plane shear distortions and transform as E_g; and another two involve only in-plane lattice distortions and transform as B_{1g} and B_{2g}. These last two correspond to the strain fields $\varepsilon_{B_{1g}} = \partial_X U_X - \partial_Y U_Y$ and $\varepsilon_{B_{2g}} = \partial_X U_Y + \partial_Y U_X$, respectively. Note that $\mathbf{U}(\mathbf{X})$ is defined in the crystallographic unit cell.

A simple symmetry analysis reveals that the only vestigial order parameter that couples linearly to a symmetry-breaking strain mode is the nematic one, $\Phi_{B_{2g}}$, which couples to the shear mode $\varepsilon_{B_{2g}}$. Such a linear coupling drives a softening of the sound velocity of the acoustic phonon mode that propagates along the [100] direction. This coupling has been widely discussed in the literature and explored to experimentally probe both long-range nematic order and nematic fluctuations [75–82]. Because $\Phi_{B_{2u}}$ and $\Phi_{A_{2u}}$ do not couple linearly to any of the strain modes, the lattice remains tetragonal in the spin-current and charge-ordered vestigial phases.

Besides the elastic lattice modes, associated with acoustic phonons, the system also has optical phonon modes. Among those, there is an A_{2u} zone-center optical phonon, with an energy of about $\Omega_{A_{2u}} \approx 40$ meV, corresponding to an in-phase displacement Z of the Fe and As/Se atoms along the out-of-plane axis [83]. Symmetry dictates that there must be a linear coupling between this Z displacement and the vestigial order parameter $\Phi_{A_{2u}}$. Therefore, the condensation of $\Phi_{A_{2u}}$ leads to a softening of the A_{2u} optical phonon. Although the crystal structure remains tetragonal after $\Omega_{A_{2u}} \to 0$, this linear coupling opens the interesting possibility of probing fluctuations associated with the spin-current vestigial phase by inelastic neutron scattering measurements of the phonon spectrum. Furthermore, since this phonon mode is infrared active, it is in principle possible to manipulate the spin-current order parameter via pump-probe spectroscopy.

We finish this section by noting that the vestigial order parameter $\Phi_{B_{2u}}$ does not couple linearly to either acoustic or optical phonon modes. This implies that the onset of charge-ordered vestigial phase is not accompanied by any changes in the atomic positions of the crystal structure.

B. Conjugate fields and transverse fields

The analysis above reveals that the shear strain $\varepsilon_{B_{2g}}$ acts as a conjugate field to the vestigial nematic order parameter $\Phi_{B_{2g}}$. Thus, controlled application of uniaxial strain, for instance via piezoelectric devices, offers a

unique route to probe nematicity. This has been routinely employed to study nematicity in the iron pnictides and other systems that display nematic order.

An interesting question is whether there are experimentally accessible conjugate fields to the other vestigial order parameters obtained here, $\Phi_{A_{2u}}$ and $\Phi_{B_{2u}}$. Interestingly, an electric field applied along the z axis, E_z, also transforms as A_{2u}, and thus behaves as a conjugate field to the spin-current order parameter $\Phi_{A_{2u}}$. Such a field can be experimentally applied in a controlled way via electrostatic gating of thin films. It can also appear in a less controlled way due to the existence of a substrate, as is the case in FeSe grown on $SrTiO_3$ [84–89], or due to a particular feature of the crystalline structure, as is the case of the 1144 pnictides [33, 90]. The linear coupling between E_z and $\Phi_{A_{2u}}$ opens up the unexplored possibility of experimentally probing spin-current order and spin-current fluctuations in a systematic way.

It is also interesting to note that the order parameters $\Phi_{A_{2u}}$ and $\Phi_{B_{2g}}$ are not completely unrelated, as they live in the same two-dimensional subspace spanned by the two-component magnetic order parameter $\boldsymbol{\eta}_1$ (or $\boldsymbol{\eta}_2$). This is a direct consequence of the common vestigial nature of both orders, and manifested clearly in Eq. (9): while $\Phi_{B_{2g}}$ is associated with the τ^z Pauli matrix living in the "Bloch sphere" set by the the two components of $\boldsymbol{\eta}_1$, $\Phi_{A_{2u}}$ is described in terms of the τ^x Pauli matrix. In view of the standard commutation relations between Pauli matrices, it is expected that one of the order parameters acts effectively as a "transverse field" to the other one. Of course, this by itself does not imply that non-trivial Berry phases appear in the free energy (for an analysis related to the simpler case of orbital nematicity, see Ref. 49). Yet, it does suggest that the conjugate field to $\Phi_{A_{2u}}$ will have an effect on $\Phi_{B_{2g}}$ (and vice-versa), as they live in the same subspace. Thus, an electric field E_z may be used to tune the nematic transition, instead of shear strain. The advantage is that the former does not explicitly break the symmetry that is spontaneously broken by $\Phi_{B_{2g}}$. This effect, which we dub *electro-nematic*, is unique to the vestigial nature of the nematic order, and would not be present if nematicity was simply a manifestation of ferro-orbital order, see Ref. 49.

As for the vestigial order parameter $\Phi_{B_{2u}}$, we did not identify a simple experimentally accessible quantity that could act as its conjugate field. It is possible, however, to combine two different quantities whose product transforms as B_{2u}. This is achieved for instance by combining a biaxial strain $\varepsilon_{B_{1g}}$ and a perpendicular electric field E_z. Since $B_{1g} \otimes A_{2u} = B_{2u}$, there is a trilinear coupling between $\Phi_{B_{2u}}$, $\varepsilon_{B_{1g}}$, and E_z. Of course, the disadvantage of this trilinear coupling is that E_z also induces $\Phi_{A_{2u}}$.

C. Intertwinment with Néel antiferromagnetic order

The magnetically ordered states discussed in our work, described in terms of the order parameters $\boldsymbol{\eta}_\alpha$, are associated with the ordering vectors $(\pi, 0)$ and $(0, \pi)$ of the Fe-only Brillouin zone. Another type of magnetic order that has been observed in certain hole-doped iron pnictides is the well-known Néel order, described by an order parameter $\mathbf{N}$, and associated with the ordering vector (π, π) of the Fe-only Brillouin zone [91]. Of course, in the crystallographic Brillouin zone, (π, π) is folded onto $(0, 0)$. But the key point is that, because $(\pi, \pi) = (\pi, 0) + (0, \pi)$, one expects that $\mathbf{N}$ will couple to a bilinear combination of $\eta^\mu_\alpha \eta^\nu_\alpha$, with $\mu \neq \nu$. Those are precisely the vestigial order parameters defined in Eq. (9).

This simple observation motivates us to investigate the coupling between the Néel order parameter $\mathbf{N}$ and the vestigial order parameters Φ. To ensure time-reversal invariance, since $\mathbf{N}$ is odd under time-reversal whereas Φ is even, this coupling can only take place in the presence of an external magnetic field $\mathbf{H}$. Note that $\mathbf{H}$ is a pseudo-vector whose out-of-plane component transforms as A_{2g} and whose in-plane components transform as E_g [40]. In contrast, for the Néel order on the Fe-sites, $\mathbf{N}$, $(N_x, -N_y)^T$ forms an E_u doublet while N_z transforms as B_{1u}. A symmetry analysis reveals that there is no trilinear coupling involving $\mathbf{H}$, $\mathbf{N}$, and the vestigial nematic order parameter $\Phi_{B_{2g}}$.

The situation is different for the vestigial order parameter $\Phi_{B_{2u}}$. The free energy in such a case allows for a trilinear coupling of the form:

$$\mathcal{F}_{B_{2u}} = \lambda_{B_{2u}} \Phi_{B_{2u}} \mathbf{H} \cdot \mathbf{N} \,, \tag{25}$$

where $\lambda_{B_{2u}}$ is a coupling constant. The physical implication of this term is clear: in the vestigial charge-orderd phase, where $\Phi_{B_{2u}} \neq 0$, application of a uniform magnetic field induces Néel order polarized parallel to the field direction. Because $\mathbf{H}$ inevitably induces ferromagnetic order, the resulting magnetic configuration is *ferrimagnetic*, as illustrated in Fig. 7.

A trilinear coupling is also allowed in the case of the vestigial order parameter $\Phi_{A_{2u}}$, although its form is different than that of Eq. (25):

$$\mathcal{F}_{A_{2u}} = \lambda_{A_{2u}} \Phi_{A_{2u}} \left(H_x N_y + H_y N_x \right) \,, \tag{26}$$

where $\lambda_{A_{2u}}$ denotes a coupling constant. Here, the subscripts x, y refer to the 1-Fe unit cell, i.e. they are parallel to the Fe-Fe nearest-neighbor directions. In the spin-current phase, where $\Phi_{A_{2u}} \neq 0$, the polarization of the Néel order induced by the external field depends crucially on its direction. An out-of-plane field, for instance, does not induce any Néel order, as illustrated in Fig. 7. On the other hand, for $\mathbf{H} \parallel \hat{\mathbf{x}}$ or $\mathbf{H} \parallel \hat{\mathbf{y}}$, the Néel order parameter is polarized along the perpendicular in-plane

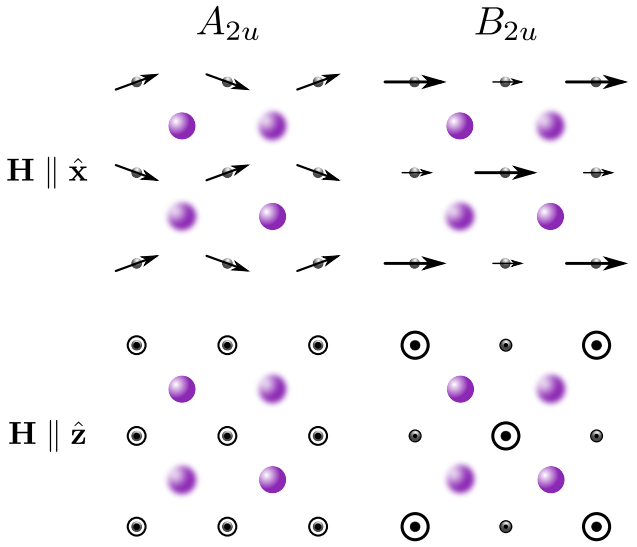

Figure 7. Illustration of the induced magnetic configurations in the A_{2u} and B_{2u} paramagnetic vestigial phases induced by the presence of an external magnetic field $\mathbf{H}$. Besides the usually induced ferromagnetic order, Néel order is also induced in this case, resulting in ferrimagnetic or canted antiferromagnetic configurations. For out-of-plane fields, currents are induced around the As/Se atoms. These are omitted in the figure.

direction, $\mathbf{N} \parallel \hat{\mathbf{y}}$ or $\mathbf{N} \parallel \hat{\mathbf{x}}$, respectively. Due to the additional parallel ferromagnetic component induced by $\mathbf{H}$, the resulting magnetic configuration is that of a *canted antiferromagnet* (see Fig. 7). The relative angle $\Delta\theta$ between the ferromagnetic and Néel components that are induced by an in-plane magnetic field applied along a direction that makes an angle $\theta_{\rm H}$ with the x axis is given by:

$$\Delta\theta = 2\theta_{\rm H} \pm \frac{\pi}{2}$$

where the $\pm$ sign depends on the sign of the coupling constant $\lambda_{A_{2u}}$. Clearly, for $\theta_{\rm H} = \pm\frac{\pi}{4}$, corresponding to a field applied along the (anti)diagonal, there is no canting and the induced order is ferrimagnetic, similarly to the case with $\Phi_{B_{2u}}$ order.

We dub the rather unusual effect described by Eqs. (25)-(26) of Néel order being induced by a uniform magnetic field the *ferro-Néel effect.* Its existence highlights the non-trivial paramagnetic character of the vestigial phases. It provides yet another possible route to experimentally probe the vestigial spin-current and charge-ordered phases. The key manifestation, which can be probed by neutron scattering experiments, would be the emergence of a magnetic Bragg peak at (π, π) (of the 1-Fe Brillouin zone) upon application of a magnetic field.

V. IMPACT OF THREE-DIMENSIONALITY: CONTRASTING 122 AND 1111, 111, 11 COMPOUNDS

The results derived in this work refer to the space group $P4/nmm$, for which the crystallographic unit cell only contains a single FeAs/Se layer. Because the materials are layered compounds, the stacking pattern of the layers is crucial to determine the applicability of our results to the different families of iron-based superconductors. In the case where the layers are simply stacked on top of each other, as is the case in the 1111, 111, and 11 compounds (such as LaFeAsO, NaFeAs, and FeSe, respectively), the space group is indeed $P4/nmm$. Consequently, all results derived here apply directly to these systems. Specifically, the vestigial ordered states have ordering vectors $\mathbf{Q} = (0, 0, 0)$ in the crystallographic Brillouin zone. This also implies that the Néel order parameter of Sec. IV C has an ordering vector $(\pi, \pi, 0)$ in the 1-Fe Brillouin zone.

The situation changes qualitatively in the case of the 122 compounds (e.g. $BaFe_2As_2$), where the layers are stacked in a staggered pattern. In this case, the appropriate space group is not the non-symmorphic $P4/nmm$ group but instead the symmorphic $I4/mmm$. While a full group-theoretical analysis is beyond the scope of this work, we can still determine the main qualitative changes in our results in this case. This can be accomplished by starting from the artificial 1-Fe Brillouin zone and noting that the main difference between the compounds with $P4/nmm$ and $I4/mmm$ space groups is on the z-component of the momentum vector $\mathbf{P}_{\rm fold}$ responsible for folding the larger 1-Fe Brillouin zone onto the crystallographic 2-Fe Brillouin zone [61, 62, 92]. In particular, for the compounds with $P4/nmm$ space group, the folding vector is $\mathbf{P}_{\rm fold} = (\pi, \pi, 0)$ whereas for the compounds with $I4/nmm$ space group, it is $\mathbf{P}_{\rm fold} = (\pi, \pi, \pi)$. Using these folding vectors, the wave-vector in the crystallographic unit cell can be written as $\mathbf{Q} = \hat{\mathbf{R}}_{\pi/4} \cdot (\mathbf{q} + \mathbf{P}_{\rm fold})$, where $\mathbf{q}$ is the wave-vector in the 1-Fe Brillouin zone and $\hat{\mathbf{R}}_{\pi/4}$ realizes a 45° rotation around the $\hat{\mathbf{z}}$-axis (see Fig. 2).

Because the vestigial nematic order parameter $\Phi_{B_{2g}}$ has ordering vector $\mathbf{q} = (0, 0, 0)$ in the 1-Fe Brillouin zone, it remains a zero wave-vector order in the 2-Fe Brillouin zone for both types of systems. Thus, in regards to the nematic phase, the results are the same for both $P4/nmm$ and $I4/mmm$ compounds. On the other hand, the 1-Fe Brillouin zone ordering vector of the two other vestigial order parameters $\Phi_{A_{2u}}$ and $\Phi_{B_{2u}}$ is $\mathbf{q} = (\pi, \pi, 0)$. This means that, in the 2-Fe (crystallographic) Brillouin zone, the ordering vector is $\mathbf{Q} = (0, 0, 0)$ for the $P4/nmm$ compounds, but $\mathbf{Q} = (0, 0, \pi)$ for the $I4/mmm$ compounds. Consequently, these vestigial orders break translational symmetry by doubling the periodicity along the z direction. While this property provides another experimentally accessible way of detecting these vestigial orders (e.g. via X-ray scattering), it also implies that E_z is not a

conjugate field for $\Phi_{A_{2u}}$ and that A_{2u} spin-current order is not accompanied by a soft zone-center phonon. The results for the coupling to the Néel order parameter of Sec. IV C remain the same, since the ordering vector of latter in the 1-Fe Brillouin zone is $(\pi, \pi, 0)$.

We finish this section by emphasizing that the premise of our framework is that the dominant magnetic fluctuations are peaked at $(\pi, 0, \pi)$ and $(0, \pi, \pi)$ in the 1-Fe Brillouin zone, i.e. they are stripe-like magnetic fluctuations. Although this is the situation in the majority of iron-based materials, this is not the case for all of them. The prime example is the 11 compound FeTe, which displays double-stripe magnetic order, with ordering vector $\left(\frac{\pi}{2}, \frac{\pi}{2}, \pi\right)$ in the 1-Fe Brillouin zone [93–95]. While our results are not relevant for that compound, this type of magnetic order does support its own set of vestigial orders, as discussed in Ref. 96. These vestigial orders have been invoked to explain the phase diagram of a related Ti-based oxypnictide [96]. We also emphasize that, in FeSe and related intercalated systems, even though the dominant magnetic fluctuations are stripe-type [97, 98], it remains widely debated whether the nematic phase is a vestigial order or the consequence of a separate instability [51, 55, 68–70, 99]. The main evidence against a simple vestigial scenario is that the low-energy magnetic fluctuations, as measured by NMR, are rather weak above the onset of nematic order [cite Bohmer]. Typically, vestigial order is triggered by the correlation length of the primary order reaching an often large threshold value [7]. Moreover, the fact that upon application of pressure the nematic transition temperature is suppressed whereas the magnetic transition temperature is enhanced [34] suggests a scenario of competing phases rather than intertwined vestigial phases. However, as shown by the first-principle calculations of Ref. 51, the magnetic ground state of FeSe seems to be much more degenerate than $(\pi, 0)$ and $(0, \pi)$ (in the 1Fe BZ). Instead, there is a family of nearly degenerate magnetic states with different ordering vectors. What they have in common is that they all support a vestigial nematic phase, despite directly competing for different magnetic configurations. This suggests an interesting case of vestigial order being stabilized over a wider temperature range by multiple competing magnetic instabilities; as such, this scenario certainly deserves further investigation.

VI. DISCUSSION AND CONCLUSIONS

In this paper we presented a simple, yet powerful framework that provides a unifying description of the complexity of the underdoped phase diagram of the iron pnictides. Such a framework consists both of primary phases that display long-range magnetic order and of their vestigial phases that intertwine spin and orbital degrees of freedom. A plethora of electronic orders that break different symmetries of the FeAs/Se layer while displaying comparable transition temperatures emerge within this framework, from stripe magnetic order and nematicity to C_4 magnetism, charge order, and loop spin-current order. Formally, all these states arise from the condensation of the symmetry-allowed simple and composite order parameters formed by the six components of the super-vector $\boldsymbol{\mathcal{M}}$ in Eq. (3), as schematically shown in Fig. 1.

Whereas previous works focusing on the idealized Fe-only square lattice have identified some of these phases, all electronic orders discussed here respect the symmetries of the crystallographic non-symmorphic space group that describes the FeAs/Se layer. These symmetries qualitatively change the nature of the vestigial phases, and the orbital-order patterns that accompany the composite spin orders. Besides the widely investigated Ising-nematic order parameter $\Phi_{B_{2g}}$, which transforms as the B_{2g} irrep of the tetragonal group, two additional Ising-like, zero wave-vector composite order parameters are found, transforming as the A_{2u} and B_{2u} irreps (denoted by $\Phi_{A_{2u}}$ and $\Phi_{B_{2u}}$).

While $\Phi_{B_{2g}}$ is associated with a combination of onsite- and bond-orbital orders involving the d_{xz}, d_{yz}, d_{xy} orbitals, $\Phi_{A_{2u}}$ is accompanied by spin-current order involving the d_{xy} orbitals and staggered d_{xz}/d_{yz} orbital hybridization. Similarly, $\Phi_{B_{2u}}$ is accompanied by checkerboard charge-order related to the d_{xy} orbitals and staggered d_{xz}/d_{yz} spin-orbit coupling. Moreover, the onset of $\Phi_{A_{2u}}$ and $\Phi_{B_{2u}}$ also triggers different types of Rashba-like and Dresselhaus-like spin-orbit couplings involving the d_{xz}/d_{yz} orbitals. Importantly, these spin-orbit coupling terms are a consequence of a spontaneous symmetry breaking driven by magnetic fluctuations, rather than an explicit broken symmetry due to e.g. a substrate or an applied electric field.

These rather unusual orbital patterns lead to a variety of interesting effects unveiled in our work: the lifting of the spin-degeneracy of the electronic band structure in the vestigial A_{2u} and B_{2u} phases; the electro-nematic effect, by which an electric field applied perpendicular to the FeAs/Se layer acts effectively as a transverse field to the nematic order parameter; and the ferro-Néel effect, describing the fact that Néel order is induced by a uniform magnetic field in the vestigial A_{2u} and B_{2u} phases, resulting in ferrimagnetic and canted antiferromagnetic spin configurations.

The most promising iron-based compounds where these unusual A_{2u} and B_{2u} vestigial phases may be realized are those for which the primary C_4 magnetic phases have been observed. Interestingly, not only doping, but also pressure, have been shown to be capable of tuning the magnetic ground state from stripe to C_4 [34, 36]. Recently, indirect evidence for charge-order, presumably due to a non-zero $\Phi_{B_{2u}}$, has been reported in ARPES experiments in hole-doped compounds [101]. Although the experiment was performed inside the charge-spin density-wave phase, it would be interesting to investigate whether the effect persists into the paramagnetic phase. In the 1144 compound, it has been argued that a non-zero $\Phi_{A_{2u}}$

exists due to a small symmetry-breaking field associated with the crystal structure of this material, combined with proximity to a spin-vortex magnetic phase [33].

More broadly, the formalism discussed here could also be relevant to other correlated systems that have the same space group as the iron pnictides and display magnetic or nematic orders. One interesting case is that of URu_2Si_2, which has the same $I4/mmm$ space group as the 122 pnictides. Nematic order has been suggested below the hidden-order temperature by certain experiments, which may be an instability on its own right or a B_{2g} vestigial phase [102, 103]. Other experiments indicate non-magnetic Fermi surface folding with ordering vector $(0, 0, \pi)$ in the hidden-order phase, which one may speculate to be related to a A_{2u} or B_{2u} vestigial order [74, 104]. Another potentially relevant $5f$-electron system is the compound $CeAuSb_2$, whose space group $P4/nmm$ is the same as the 11, 111, and 1111 pnictides. Recent neutron scattering experiments revealed a change in the magnetic ground state from single-$\mathbf{Q}$ stripe to double-$\mathbf{Q}$ magnetic order as function of an applied magnetic field [105]. Whether vestigial phases also emerge in this phase diagram remains to be established.

ACKNOWLEDGMENTS

The authors are grateful to W. R. Meier for inspiring discussions on the group-theoretical description of iron pnictides. The authors further acknowledge fruitful discussions with C. Batista, E. Berg, P. Canfield, A. Chubukov, S. Kivelson, A. Kreyssig, P. Orth, J. Schmalian, and R. Valentí. This work was supported by the U.S. Department of Energy, Office of Science, Basic Energy Sciences, under Award number DE-SC0012336.

Appendix A: Low-energy electronic model

For completeness, we here provide the details of the non-interacting Hamiltonian used to obtain the band structures shown in Figs. 4–6. They follow the parametrization first proposed in Ref. 40. Note that the results presented in the main text are independent on the specific form of the Hamiltonian, since all the arguments are based on symmetry. The basis used here and throughout the paper is

$$\Psi_s(\mathbf{K}) = \begin{pmatrix} \Psi_{M_+,s}(\mathbf{K}+\mathbf{Q}_M) \\ \Psi_{M_-,s}(\mathbf{K}+\mathbf{Q}_M) \\ \Psi_{\Gamma,s}(\mathbf{K}) \end{pmatrix} , \tag{A1}$$

where $\Psi_{\Gamma,s}$ and $\Psi_{M,s}$ are given in Eqs. (12) and (13). The Hamiltonian is given by:

$$\mathcal{H} = \begin{pmatrix} h_+(\mathbf{K}) & h_{+-}^{\rm SOC} & 0 \\ (h_{+-}^{\rm SOC})^\dagger & h_-(\mathbf{K}) & 0 \\ 0 & 0 & h_\Gamma(\mathbf{K}) + h_\Gamma^{\rm SOC} \end{pmatrix} . \tag{A2}$$

Recall that $\mathbf{K}$ labels momentum in the crystallographic 2-Fe Brillouin zone and $\mathbf{Q}_M = (\pi, \pi)$. $\mathcal{H}$ is a 12×12 matrix with components

$$\begin{aligned} &h_\pm(\mathbf{K}) = \\ &\begin{pmatrix} \epsilon_1 + \frac{\mathbf{K}^2}{2m_1} \pm a_1 K_x K_y & -iv_\pm(\mathbf{K}) \\ iv_\pm(\mathbf{K}) & \epsilon_3 + \frac{\mathbf{K}^2}{2m_3} \pm a_3 K_x K_y \end{pmatrix} \otimes \sigma^0 , \\ &h_\Gamma(\mathbf{K}) = \\ &\begin{pmatrix} \epsilon_\Gamma + \frac{\mathbf{K}^2}{2m_\Gamma} + bK_x K_y & c(K_x^2 - K_y^2) \\ c(K_x^2 - K_y^2) & \epsilon_\Gamma + \frac{\mathbf{K}^2}{2m_\Gamma} - bK_x K_y \end{pmatrix} \otimes \sigma^0 , \end{aligned} \tag{A3}$$

where

$$\begin{aligned} v_\pm(\mathbf{K}) = v(\pm K_x + K_y) + p_1(\pm K_X^3 + K_y^3) \\ + p_2 K_x K_y (K_x \pm K_y) , \end{aligned} \tag{A4}$$

and the SOC components are

$$\begin{aligned} h_\Gamma^{\rm SOC} &= \frac{1}{2}\lambda_\Gamma \begin{pmatrix} 0 & -i \\ i & 0 \end{pmatrix} \otimes \sigma^3 , \\ h_{+-}^{\rm SOC} &= \frac{i}{2}\lambda_M \left[\begin{pmatrix} 0 & 1 \\ 0 & 0 \end{pmatrix} \otimes \sigma^1 + \begin{pmatrix} 0 & 0 \\ 1 & 0 \end{pmatrix} \otimes \sigma^2 \right] . \end{aligned} \tag{A5}$$

The parameters can be determined on a case-by-case basis by fitting to tight-binding results. For concreteness, we adopted the ones provided in Ref. 40, based on the band structure of Ref. 106. For the plots in Figs. 4, 5, and 6, we set $\lambda_\Gamma = \lambda_M = 75$meV to make the SOC effects more pronounced. For the momentum independent fermionic bilinears we set $\Delta_{B_{2g}}^{(1,2)} = \Delta_{A_{2u}}^{(1,2)} = \Delta_{B_{2u}}^{(1,2)} = 100$meV to ensure a more pronounced effect. For the Rashba- and Dresselhaus-like SOC terms, we set $\Delta_{A_{2u}}^{(3,4,5,6)} = \Delta_{B_{2u}}^{(3,4,5,6)} = 10$meV.

Appendix B: Fermionic bilinears transforming as A_{2u} and B_{2u}

Here we present the fermionic bilinears constructed from the electronic operator (A1) that transform as the A_{2u} and B_{2u} irreps, and are thus induced by the onset of $\Phi_{A_{2u}}$ and $\Phi_{B_{2u}}$. We use Eqs. (12) and (13) to express the bilinears in terms of the orbital operators with momentum defined in the 1-Fe Brillouin zone. Note that the bilinears that transform as B_{2g} have been previously discussed in Ref. 67.

1. Electron pockets

We first focus on bilinears of the form $\left\langle \Psi_{M_\pm}^\dagger \hat{\Lambda} \Psi_{M_\pm} \right\rangle$, which involve states at the electron pockets. The vertex $\hat{\Lambda}$ has spin, orbital and momentum parts, $\hat{\Lambda} = \hat{\Lambda}^{(s)} \otimes \hat{\Lambda}^{(o)} \otimes \hat{\Lambda}^{(k)}$. In the case of spin- and momentum-independent bilinears, $\hat{\Lambda}^{(s)}$ and $\hat{\Lambda}^{(k)}$ are identity matrices and the orbital vertex $\hat{\Lambda}^{(o)}$ must transform according to

the A_{2u} and B_{2u} irreps. Using the vertices tabulated in Ref. 40, we find:

$$\Delta^{(1)}_{A_{2u}} = \left\langle d^\dagger_{xz,s}(\mathbf{k}+\mathbf{Q}_2) d_{yz,s}(\mathbf{k}+\mathbf{Q}_1)\right\rangle .$$
$$\Delta^{(1)}_{B_{2u}} = \left\langle d^\dagger_{xz,s}(\mathbf{k}+\mathbf{Q}_2) d_{yz,s}(\mathbf{k}+\mathbf{Q}_1)\right\rangle . \quad \text{(B1)}$$

In this expression and hereafter, sums over momentum and spin indices are left implicit. In addition to these terms, that are also bilinears that are not spin diagonal. Consider first the case $\hat{\Lambda}^{(s)} = \sigma^z$, discussed in the main text. Since σ^z transforms as A_{2g}, all we need is to find the orbital vertices $\hat{\Lambda}^{(o)}$ that transform as A_{1u} and B_{1u}, since $A_{2g}\otimes A_{1u} = A_{2u}$ and $A_{2g}\otimes B_{1u} = B_{2u}$. We obtain:

$$\Delta^{(2)}_{A_{2u}} = i\left\langle d^\dagger_{xy,s}(\mathbf{k}+\mathbf{Q}_2)\sigma^z_{ss'} d_{xy,s'}(\mathbf{k}+\mathbf{Q}_1) - \text{h.c.}\right\rangle ,$$
$$\Delta^{(2)}_{B_{2u}} = i\left\langle d^\dagger_{xz,s}(\mathbf{k}+\mathbf{Q}_2)\sigma^z_{ss'} d_{yz,s'}(\mathbf{k}+\mathbf{Q}_1) - \text{h.c.}\right\rangle . \quad \text{(B2)}$$

Note that the imaginary prefactor i ensures that time-reversal symmetry is preserved. We can also construct momentum-independent bilinears with the spin-vertex $\hat{\Lambda}^{(s)} = (\sigma^x, \sigma^y)$, which transforms as E_g, and orbital vertices $\hat{\Lambda}^{(o)} \sim E_u$. The result is

$$\begin{aligned}\Delta^{(7)}_{A_{2u}} &= i\left\langle d^\dagger_{xy,s}(\mathbf{k}+\mathbf{Q}_1)\sigma^y_{ss'} d_{xz,s'}(\mathbf{k}+\mathbf{Q}_2) - \text{h.c.}\right\rangle \\ &\quad - i\left\langle d^\dagger_{xy,s}(\mathbf{k}+\mathbf{Q}_2)\sigma^x_{ss'} d_{yz,s'}(\mathbf{k}+\mathbf{Q}_1) - \text{h.c.}\right\rangle \\ \Delta^{(7)}_{B_{2u}} &= i\left\langle d^\dagger_{xy,s}(\mathbf{k}+\mathbf{Q}_1)\sigma^x_{ss'} d_{xz,s'}(\mathbf{k}+\mathbf{Q}_2) - \text{h.c.}\right\rangle \\ &\quad - i\left\langle d^\dagger_{xy,s}(\mathbf{k}+\mathbf{Q}_2)\sigma^y_{ss'} d_{yz,s'}(\mathbf{k}+\mathbf{Q}_1) - \text{h.c.}\right\rangle . \end{aligned} \quad \text{(B3)}$$

These terms are very similar to the regular SOC terms that are present even in the absence of vestigial order. However, the momentum dependence differs, which results in a staggered SOC, similar to $\Delta^{(2)}_{A_{2u}}$.

2. Hole pockets

We now turn to the bilinears involving states at the hole pockets, which have the form $\left\langle \Psi^\dagger_\Gamma \hat{\Lambda}\, \Psi_\Gamma \right\rangle$. As before, we write the vertex as $\hat{\Lambda} = \hat{\Lambda}^{(s)}\otimes\hat{\Lambda}^{(o)}\otimes\hat{\Lambda}^{(k)}$. The doublet Ψ_Γ, corresponding to d_{xz} and d_{yz} orbitals, transforms as the E_g irrep of the $P4/nmm$ group at Γ. Thus, the momentum-independent bilinears constructed from such fermions will transform as one of the *gerade* irreps:

$$E_g \otimes E_g = A_{1g}\otimes A_{2g}\otimes B_{1g}\otimes B_{2g} . \quad \text{(B4)}$$

To construct fermionic bilinears transforming as *ungerade* irreps it is necessary to consider vertices $\hat{\Lambda}^{(s)}$ and $\hat{\Lambda}^{(k)}$ that are odd under inversion. Since spin-vertices are even under inversion, the vertices that are odd under inversion must be $\hat{\Lambda}^{(k)}$, which must be odd in momentum. Hence, to preserve time-reversal symmetry, the spin vertices $\hat{\Lambda}^{(s)}$ therefore cannot be the identity. We thus construct the allowed vertices by combining (k_x, k_y), which transforms as E_u, and (σ^x, σ^y), which transforms as E_g:

$$E_u \otimes E_g = A_{1u}\otimes A_{2u}\otimes B_{1u}\otimes B_{2u} . \quad \text{(B5)}$$

Combining Eqs. (B4) and (B5) gives:

$$E_g\otimes E_g\otimes E_u\otimes E_g = 4A_{1u}\otimes 4A_{2u}\otimes 4B_{1u}\otimes 4B_{2u} , \quad \text{(B6)}$$

The numerical prefactors denote how many copies of the respective irreps can be constructed. The 4 different A_{2u} terms result from

$$\begin{aligned} &A_{1g}\otimes A_{2u}\\ &A_{2g}\otimes A_{1u}\\ &B_{1g}\otimes B_{2u}\\ &B_{2g}\otimes B_{1u} , \end{aligned} \quad \text{(B7)}$$

whereas the 4 different B_{2u} terms are:

$$\begin{aligned} &A_{1g}\otimes B_{2u}\\ &A_{2g}\otimes B_{1u}\\ &B_{1g}\otimes A_{2u}\\ &B_{2g}\otimes A_{1u} . \end{aligned} \quad \text{(B8)}$$

In the expressions above, the *gerade* irreps originate from the bilinear $\Psi^\dagger_\Gamma\Psi_\Gamma$, Eq. (B4), whereas the *ungerade* irreps come $\hat{\Lambda} = \hat{\Lambda}^{(s)}\otimes\hat{\Lambda}^{(k)}$, Eq. (B5). Writing down these combinations explicitly, we have

$$\begin{aligned} [A_{1g}] &\sim d^\dagger_{xz,s}(\mathbf{k}) d_{xz,s'}(\mathbf{k}) + d^\dagger_{yz,s}(\mathbf{k}) d_{yz,s'}(\mathbf{k})\\ [A_{2g}] &\sim d^\dagger_{xz,s}(\mathbf{k}) d_{yz,s'}(\mathbf{k}) - d^\dagger_{yz,s}(\mathbf{k}) d_{xz,s'}(\mathbf{k})\\ [B_{1g}] &\sim d^\dagger_{xz,s}(\mathbf{k}) d_{yz,s'}(\mathbf{k}) + d^\dagger_{yz,s}(\mathbf{k}) d_{xz,s'}(\mathbf{k})\\ [B_{2g}] &\sim d^\dagger_{xz,s}(\mathbf{k}) d_{xz,s'}(\mathbf{k}) - d^\dagger_{yz,s}(\mathbf{k}) d_{yz,s'}(\mathbf{k}) . \end{aligned} \quad \text{(B9)}$$

Moreover:

$$\begin{aligned} [A_{1u}] &\sim k_x\sigma^x_{ss'} + k_y\sigma^y_{ss'}\\ [A_{2u}] &\sim k_x\sigma^y_{ss'} - k_y\sigma^x_{ss'}\\ [B_{1u}] &\sim k_x\sigma^y_{ss'} + k_y\sigma^x_{ss'}\\ [B_{2u}] &\sim k_x\sigma^x_{ss'} - k_y\sigma^y_{ss'} . \end{aligned} \quad \text{(B10)}$$

In the expressions above, the orbitals, spins, and momenta, are defined with respect to the coordinate system of the single Fe atom square lattice. Combining these expressions according to Eqs. (B7) and (B8) gives:

$$\begin{aligned} \Delta^{(3)}_{A_{2u}} &\sim \left\langle (k_x\sigma^y_{ss'} - k_y\sigma^x_{ss'}) \right.\\ &\qquad \left. \left(d^\dagger_{xz,s}(\mathbf{k}) d_{xz,s'}(\mathbf{k}) + d^\dagger_{yz,s}(\mathbf{k}) d_{yz,s'}(\mathbf{k})\right)\right\rangle \\ \Delta^{(4)}_{A_{2u}} &\sim \left\langle (k_x\sigma^x_{ss'} + k_y\sigma^y_{ss'}) \right.\\ &\qquad \left. \left(d^\dagger_{xz,s}(\mathbf{k}) d_{yz,s'}(\mathbf{k}) - d^\dagger_{yz,s}(\mathbf{k}) d_{xz,s'}(\mathbf{k})\right)\right\rangle \\ \Delta^{(5)}_{A_{2u}} &\sim \left\langle (k_x\sigma^x_{ss'} - k_y\sigma^y_{ss'}) \right.\\ &\qquad \left. \left(d^\dagger_{xz,s}(\mathbf{k}) d_{yz,s'}(\mathbf{k}) + d^\dagger_{yz,s}(\mathbf{k}) d_{xz,s'}(\mathbf{k})\right)\right\rangle \\ \Delta^{(6)}_{A_{2u}} &\sim \left\langle (k_x\sigma^y_{ss'} + k_y\sigma^x_{ss'}) \right.\\ &\qquad \left. \left(d^\dagger_{xz,s}(\mathbf{k}) d_{xz,s'}(\mathbf{k}) - d^\dagger_{yz,s}(\mathbf{k}) d_{yz,s'}(\mathbf{k})\right)\right\rangle \end{aligned} \quad \text{(B11)}$$

for A_{2u} and

$$\begin{aligned}
\Delta^{(3)}_{B_{2u}} &\sim \big\langle\, (k_x\sigma^x_{ss'} - k_y\sigma^y_{ss'}) \\
&\qquad \big(d^\dagger_{xz,s}(\mathbf{k})d_{xz,s'}(\mathbf{k}) + d^\dagger_{yz,s}(\mathbf{k})d_{yz,s'}(\mathbf{k})\big) \,\big\rangle \\
\Delta^{(4)}_{B_{2u}} &\sim \big\langle\, (k_x\sigma^y_{ss'} + k_y\sigma^x_{ss'}) \\
&\qquad \big(d^\dagger_{xz,s}(\mathbf{k})d_{yz,s'}(\mathbf{k}) - d^\dagger_{yz,s}(\mathbf{k})d_{xz,s'}(\mathbf{k})\big) \,\big\rangle \\
\Delta^{(5)}_{B_{2u}} &\sim \big\langle\, (k_x\sigma^y_{ss'} - k_y\sigma^x_{ss'}) \\
&\qquad \big(d^\dagger_{xz,s}(\mathbf{k})d_{yz,s'}(\mathbf{k}) + d^\dagger_{yz,s}(\mathbf{k})d_{xz,s'}(\mathbf{k})\big) \,\big\rangle \\
\Delta^{(6)}_{B_{2u}} &\sim \big\langle\, (k_x\sigma^x_{ss'} + k_y\sigma^y_{ss'}) \\
&\qquad \big(d^\dagger_{xz,s}(\mathbf{k})d_{xz,s'}(\mathbf{k}) - d^\dagger_{yz,s}(\mathbf{k})d_{yz,s'}(\mathbf{k})\big) \,\big\rangle
\end{aligned} \tag{B12}$$

for B_{2u}.

[1] B. Keimer, S. A. Kivelson, M. R. Norman, S. Uchida, and J. Zaanen. *From quantum matter to high-temperature superconductivity in copper oxides*. Nature **518**, 179 (2015).

[2] E. Fradkin, S. A. Kivelson, and J. M. Tranquada. *Colloquium: Theory of intertwined orders in high temperature superconductors*. Rev. Mod. Phys. **87**, 457 (2015).

[3] A. Himeda, T. Kato, and M. Ogata. *Stripe States with Spatially Oscillating d-Wave Superconductivity in the Two-Dimensional $t-t'-J$ Model*. Phys. Rev. Lett. **88**, 117001 (2002).

[4] E. Berg, E. Fradkin, E.-A. Kim, S. A. Kivelson, V. Oganesyan, J. M. Tranquada, and S. C. Zhang. *Dynamical Layer Decoupling in a Stripe-Ordered High-T_c Superconductor*. Phys. Rev. Lett. **99**, 127003 (2007).

[5] D. F. Agterberg and H. Tsunetsugu. *Dislocations and vortices in pair-density-wave superconductors*. Nat. Phys. **4**, 639 (2008).

[6] P. A. Lee. *Amperean Pairing and the Pseudogap Phase of Cuprate Superconductors*. Phys. Rev. X **4**, 031017 (2014).

[7] R. M. Fernandes, P. P. Orth, and J. Schmalian. *Intertwined vestigial order in quantum materials: nematicity and beyond*. arXiv:1804.00818 (2018).

[8] J. Paglione and R. L. Greene. *High-temperature superconductivity in iron-based materials*. Nat. Phys. **6**, 645 (2010).

[9] D. C. Johnston. *The Puzzle of High Temperature Superconductivity in Layered Iron Pnictides and Chalcogenides*. Advances in Physics **59**, 803 (2010).

[10] P. J. Hirschfeld, M. M. Korshunov, and I. I. Mazin. *Gap symmetry and structure of Fe-based superconductors*. Rep. Prog. Phys. **74**, 124508 (2011).

[11] A. V. Chubukov. *Pairing Mechanism in Fe-Based Superconductors*. Ann. Rev. Cond. Mat. Phys. **3**, 57 (2012).

[12] S. Nandi, M. G. Kim, A. Kreyssig, R. M. Fernandes, D. K. Pratt, A. Thaler, N. Ni, S. L. Bud?ko, P. C. Canfield, J. Schmalian, R. J. McQueeney, and A. I. Goldman. *Anomalous Suppression of the Orthorhombic Lattice Distortion in Superconducting $Ba(Fe_{1-x}Co_x)_2As_2$ Single Crystals*. Phys. Rev. Lett. **104**, 057006 (2010).

[13] A. E. Böhmer and A. Kreisel. *Nematicity, magnetism and superconductivity in FeSe*. J. Phys.: Condens. Matter **30**, 023001 (2017).

[14] A. I. Coldea and M. D. Watson. *The key ingredients of the electronic structure of FeSe*. Ann. Rev. Cond. Mat. Phys. **9**, 125 (2018).

[15] F. Krüger, S. Kumar, J. Zaanen, and J. van den Brink. *Spin-orbital frustrations and anomalous metallic state in iron-pnictide superconductors*. Phys. Rev. B **79**, 054504 (2009).

[16] C.-C. Lee, W.-G. Yin, and W. Ku. *Ferro-Orbital Order and Strong Magnetic Anisotropy in the Parent Compounds of Iron-Pnictide Superconductors*. Phys. Rev. Lett. **103**, 267001 (2009).

[17] D. D. Khalyavin, S. W. Lovesey, P. Manuel, F. Kruger, S. Rosenkranz, J. M. Allred, O. Chmaissem, and R. Osborn. *Symmetry of re-entrant tetragonal phase in $Ba_{1-x}Na_xFe_2As_2$: Magnetic versus orbital ordering mechanism*. Phys. Rev. B **90**, 174511 (2014).

[18] C. Fang, H. Yao, W.-F. Tsai, J.-P. Hu, and S. A. Kivelson. *Theory of electron nematic order in LaFeAsO*. Phys. Rev. B **77**, 224509 (2008).

[19] C. Xu, M. Müller, and S. Sachdev. *Ising and spin orders in the iron-based superconductors*. Phys. Rev. B **78**, 020501(R) (2008).

[20] R. M. Fernandes, A. V. Chubukov, J. Knolle, I. Eremin, and J. Schmalian. *Preemptive nematic order, pseudogap, and orbital order in the iron pnictides*. Phys. Rev. B **85**, 024534 (2012).

[21] Y. Kamiya, N. Kawashima, and C. D. Batista. *Dimensional crossover in the quasi-two-dimensional Ising-O(3) model*. Phys. Rev. B **84**, 214429 (2011).

[22] R. M. Fernandes, A. V. Chubukov, and J. Schmalian. *What drives nematic order in iron-based superconductors?* Nat. Phys. **10**, 97 (2014).

[23] L. Fanfarillo, A. Cortijo, and B. Valenzuela. *Spin-orbital interplay and topology in the nematic phase of iron pnictides*. Phys. Rev. B **91**, 214515 (2015).

[24] S. Liang, A. Moreo, and E. Dagotto. *Nematic State of Pnictides Stabilized by Interplay between Spin, Orbital,*

and Lattice Degrees of Freedom. Phys. Rev. Lett. **111**, 047004 (2013).

[25] L. Wang, F. Hardy, A. E. Böhmer, T. Wolf, P. Schweiss, and C. Meingast. *Complex phase diagram of $Ba_{1-x}Na_xFe_2As_2$: A multitude of phases striving for the electronic entropy*. Phys. Rev. B **93**, 014514 (2016).

[26] M. G. Kim, A. Kreyssig, A. Thaler, D. K. Pratt, W. Tian, J. L. Zarestky, M. A. Green, S. L. Bud'ko, P. C. Canfield, R. J. McQueeney, and A. I. Goldman. *Antiferromagnetic ordering in the absence of structural distortion in $Ba(Fe_{1-x}Mn_x)_2As_2$*. Phys. Rev. B **82**, 220503(R) (2010).

[27] S. Avci, O. Chmaissem, J.M. Allred, S. Rosenkranz, I. Eremin, A.V. Chubukov, D.E. Bugaris, D.Y. Chung, M.G. Kanatzidis, J.-P Castellan, J.A. Schlueter, H. Claus, D.D. Khalyavin, P. Manuel, A. Daoud-Aladine, and R. Osborn. *Magnetically driven suppression of nematic order in an iron-based superconductor*. Nat. Commun. **5**, 3845 (2014).

[28] A. E. Böhmer, F. Hardy, L. Wang, T. Wolf, P. Schweiss, and C. Meingast. *Superconductivity-induced re-entrance of the orthorhombic distortion in $Ba_{1-x}K_xFe_2As_2$*. Nat. Commun. **6**, 7911 (2015).

[29] J. M. Allred, K. M. Taddei, D. E. Bugaris, M. J. Krogstad, S. H. Lapidus, D. Y. Chung, H. Claus, M. G. Kanatzidis, D. E. Brown, J. Kang, R. M. Fernandes, I. Eremin, S. Rosenkranz, O. Chmaissem, and R. Osborn. *Double-Q spin-density wave in iron arsenide superconductors*. Nat. Phys. **12**, 493 (2016).

[30] K. M. Taddei, J. M. Allred, D. E. Bugaris, S. Lapidus, M. J. Krogstad, R. Stadel, H. Claus, D. Y. Chung, M. G. Kanatzidis, S. Rosenkranz, R. Osborn, and O. Chmaissem. *Detailed magnetic and structural analysis mapping a robust magnetic C_4 dome in $Sr_{1-x}Na_xFe_2As_2$*. Phys. Rev. B **93**, 134510 (2016).

[31] F. Waßer, A. Schneidewind, Y. Sidis, S. Wurmehl, S. Aswartham, B. Büchner, and M. Braden. *Spin reorientation in $Ba_{0.65}Na_{0.35}Fe_2As_2$ studied by single-crystal neutron diffraction*. Phys. Rev. B **91**, 060505(R) (2015).

[32] K. M. Taddei, J. M. Allred, D. E. Bugaris, S. H. Lapidus, M. J. Krogstad, H. Claus, D. Y. Chung, M. G. Kanatzidis, R. Osborn, S. Rosenkranz, and O. Chmaissem. *Observation of the magnetic C_4 phase in $Ca_{1-x}Na_xFe_2As_2$ and its universality in the hole-doped 122 superconductors*. Phys. Rev. B **95**, 064508 (2017).

[33] W. R. Meier, Q.-P. Ding, A. Kreyssig, S. L. Bud'ko, A. Sapkota, K. Kothapalli, V. Borisov, R. Valentí, C. D. Batista, P. P. Orth, R. M. Fernandes, A. I. Goldman, Y. Furukawa, A. E. Böhmer, and P. C. Canfield. *Hedgehog spin-vortex crystal stabilized in a hole-doped iron-based superconductor*. npj Quantum Materials **3**, 5 (2018).

[34] A. E. Böhmer, K. Kothapalli, W. T. Jayasekara, J. M. Wilde, B. Li, A. Sapkota, B. G. Ueland, P. Das, Y. Xiao, W. Bi, J. Zhao, E. E. Alp, S. L. Bud'ko, P. C. Canfield, A. I. Goldman, and A. Kreyssig. *Distinct pressure evolution of coupled nematic and magnetic order in FeSe*. arXiv:1803.09449 (2018).

[35] E. Hassinger, G. Gredat, F. Valade, S. René de Cotret, A. Juneau-Fecteau, J.-Ph. Reid, H. Kim, M. A. Tanatar, R. Prozorov, B. Shen, H.-H. Wen, N. Doiron-Leyraud, and L. Taillefer. *Pressure-induced Fermi-surface reconstruction in the iron-arsenide superconductor $Ba_{1-x}K_xFe_2As_2$: Evidence of a phase transition inside the antiferromagnetic phase*. Phys. Rev. B **86**, 140502(R) (2012).

[36] E. Hassinger, G. Gredat, F. Valade, S. René de Cotret, O. Cyr-Choinière, A. Juneau-Fecteau, J.-Ph. Reid, H. Kim, M. A. Tanatar, R. Prozorov, B. Shen, H.-H. Wen, N. Doiron-Leyraud, and L. Taillefer. *Expansion of the tetragonal magnetic phase with pressure in the iron arsenide superconductor $Ba_{1-x}K_xFe_2As_2$*. Phys. Rev. B **93**, 144401 (2016).

[37] R. Khasanov, R. M. Fernandes, G. Simutis, Z. Guguchia, A. Amato, H. Luetkens, E. Morenzoni, X. Dong, F. Zhou, and Z. Zhao. *Magnetic tricritical point and nematicity in FeSe under pressure*. Phys. Rev. B **97**, 224510 (2018).

[38] J. Lorenzana, G. Seibold, C. Ortix, and M. Grilli. *Competing Orders in FeAs Layers*. Phys. Rev. Lett. **101**, 186402 (2008).

[39] P. M. R. Brydon, J. Schmiedt, and C. Timm. *Microscopically derived Ginzburg-Landau theory for magnetic order in the iron pnictides*. Phys. Rev. B **84**, 214510 (2011).

[40] V. Cvetkovic and O. Vafek. *Space group symmetry, spin-orbit coupling, and the low-energy effective Hamiltonian for iron-based superconductors*. Phys. Rev. B **88**, 134510 (2013).

[41] M. H. Christensen, J. Kang, B. M. Andersen, I. Eremin, and R. M. Fernandes. *Spin reorientation driven by the interplay between spin-orbit coupling and Hund's rule coupling in iron pnictides*. Phys. Rev. B **92**, 214509 (2015).

[42] J. Kang, X. Wang, A. V. Chubukov, and R. M. Fernandes. *Interplay between tetragonal magnetic order, stripe magnetism, and superconductivity in iron-based materials*. Phys. Rev. B **91**, 121104(R) (2015).

[43] X. Wang, J. Kang, and R. M. Fernandes. *Magnetic order without tetragonal-symmetry-breaking in iron arsenides: Microscopic mechanism and spin-wave spectrum*. Phys. Rev. B **91**, 024401 (2015).

[44] M. N. Gastiasoro and B. M. Andersen. *Competing magnetic double-**Q** phases and superconductivity-induced reentrance of C_2 magnetic stripe order in iron pnictides*. Phys. Rev. B **92**, 140506(R) (2015).

[45] M. H. Christensen, D. D. Scherer, P. Kotetes, and B. M. Andersen. *Role of multiorbital effects in the magnetic phase diagram of iron pnictides*. Phys. Rev. B **96**, 014523 (2017).

[46] I. Eremin and A. V. Chubukov. *Magnetic degeneracy and hidden metallicity of the spin density wave state in ferropnictides*. Phys. Rev. B **81**, 024511 (2010).

[47] R. M. Fernandes, E. Berg, and S. Kivelson. *Vestigial chiral and charge orders from bidirectional spin-density waves: Application to the iron-based superconductors*. Phys. Rev. B **93**, 014511 (2016).

[48] S. Borisenko, D. Evtushinsky, I. Morozov, S. Wurmehl, B. Büchner, A. Yaresko, T. Kim, M. Hoesch, T. Wolf, N. Zhigadlo. *Direct observation of spin-orbit coupling in iron-based superconductors*. Nat. Phys. **12**, 311 (2016).

[49] A. V. Maharaj, E. W. Rosenberg, A. T. Hristov, E. Berg, R. M. Fernandes, I. R. Fisher, and S. A. Kivelson. *Transverse fields to tune an Ising-nematic quantum phase transition*. Proc. Natl. Acad. Sci. **114**, 13430 (2017).

[50] P. Dai. *Antiferromagnetic order and spin dynamics in iron-based superconductors*. Rev. Mod. Phys. **87**, 855 (2015).

[51] J. K. Glasbrenner, I. I. Mazin, H. O. Jeschke, P. J. Hirschfeld, R. M. Fernandes, and R. Valentí. *Effect of magnetic frustration on nematicity and superconductivity in iron chalcogenides*. Nat. Phys. **11**, 953 (2015).

[52] Q. Si and E. Abrahams. *Strong Correlations and Magnetic Frustration in the High T_c Iron Pnictides*. Phys. Rev. Lett. **101**, 076401 (2008).

[53] L. de' Medici. *Hund's coupling and its key role in tuning multiorbital correlations*. Phys. Rev. B **83**, 205112 (2011).

[54] L. de' Medici, G. Giovannetti, and M. Capone. *Selective Mott Physics as a Key to Iron Superconductors*. Phys. Rev. Lett. **112**, 177001 (2014).

[55] F. Wang, S. A. Kivelson, and D.-H. Lee. *Nematicity and quantum paramagnetism in FeSe*. Nat. Phys. **11**, 959 (2015).

[56] E. Bascones, B. Valenzuela, and M. J. Calderón. Magnetic interactions in iron superconductors: A review. C. R. Physique **17**, 36 (2016).

[57] M. H. Christensen, J. Kang, B. M. Andersen, and R. M. Fernandes. *Spin-driven nematic instability of the multi-orbital Hubbard model: Application to iron-based superconductors*. Phys. Rev. B **93**, 085136 (2016).

[58] Q. Huang, Y. Qiu, Wei Bao, M. A. Green, J. W. Lynn, Y. C. Gasparovic, T. Wu, G. Wu, and X. H. Chen. *Neutron-Diffraction Measurements of Magnetic Order and a Structural Transition in the Parent $BaFe_2As_2$ Compound of FeAs-Based High-Temperature Superconductors*. Phys. Rev. Lett. **101**, 257003 (2008).

[59] C. de la Cruz, Q. Huang, J. W. Lynn, Jiying Li, W. Ratcliff II, J. L. Zarestky, H. A. Mook, G. F. Chen, J. L. Luo, N. L. Wang, and P. Dai. *Magnetic order close to superconductivity in the iron-based layered $LaO_{1-x}F_xFeAs$ systems*. Nature **453**, 899 (2008).

[60] J. Dong, H. J. Zhang, G. Xu, Z. Li, G. Li, W. Z. Hu, D. Wu, G. F. Chen, X. Dai, J. L. Luo, Z. Fang, and N. L. Wang. *Competing orders and spin-density-wave instability in $LaO_{1-x}F_xFeAs$*. Europhys. Lett. **83**, 27006 (2008).

[61] M. Tomić, H. O. Jeschke, and R. Valentí. *Unfolding of electronic structure through induced representations of space groups: Application to Fe-based superconductors*. Phys. Rev. B **90**, 195121 (2014).

[62] C.-H. Lin, T. Berlijn, L. Wang, C.-C. Lee, W.-G. Yin, and W. Ku. *One-Fe versus Two-Fe Brillouin Zone of Fe-Based Superconductors: Creation of the Electron Pockets by Translational Symmetry Breaking*. Phys. Rev. Lett. **107**, 257001 (2011).

[63] D. D. Scherer and B. M. Andersen. *Spin-Orbit Coupling and Magnetic Anisotropy in Iron-Based Superconductors*. Phys. Rev. Lett. **121**, 037205 (2018).

[64] M. H. Christensen, P. P. Orth, B. M. Andersen, and R. M. Fernandes. *Emergent magnetic degeneracy in iron pnictides due to the interplay between spin-orbit coupling and quantum fluctuations*. Phys. Rev. Lett. **121**, 057001 (2018).

[65] M. H. Christensen, P. P. Orth, B. M. Andersen, and R. M. Fernandes. *Magnetic phase diagram of the iron pnictides in the presence of spin-orbit coupling: Frustration between C_2 and C_4 magnetic phases*. Phys. Rev. B **98**, 014523 (2018).

[66] T. Kissikov, R. Sarkar, M. Lawson, B. T. Bush, E. I. Timmons, M. A. Tanatar, R. Prozorov, S. L. Bud'ko, P. C. Canfield, R. M. Fernandes, and N. J. Curro. *Uniaxial strain control of spin-polarization in multicomponent nematic order of $BaFe_2As_2$*. Nat. Commun. **9**, 1058 (2018).

[67] R. M. Fernandes and O. Vafek. *Distinguishing spin-orbit coupling and nematic order in the electronic spectrum of iron-based superconductors*. Phys. Rev. B **90**, 214514 (2014).

[68] A. V. Chubukov, M. Khodas, and R. M. Fernandes. *Magnetism, Superconductivity, and Spontaneous Orbital Order in Iron-Based Superconductors: Which Comes First and Why?* Phys. Rev. X **6**, 041045 (2016).

[69] Y. Yamakawa, S. Onari, and H. Kontani. *Nematicity and Magnetism in FeSe and Other Families of Fe-Based Superconductors*. Phys. Rev. X **6**, 021032 (2016).

[70] L. Fanfarillo, J. Mansart, P. Toulemonde, H. Cercellier, P. Le Fèvre, F. Bertran, B. Valenzuela, L. Benfatto, and V. Brouet. *Orbital-dependent Fermi surface shrinking as a fingerprint of nematicity in FeSe*. Phys. Rev. B **94**, 155138 (2016).

[71] Y. Suzuki, T. Shimojima, T. Sonobe, A. Nakamura, M. Sakano, H. Tsuji, J. Omachi, K. Yoshioka, M. Kuwata-Gonokami, T. Watashige, R. Kobayashi, S. Kasahara, T. Shibauchi, Y. Matsuda, Y. Yamakawa, H. Kontani, and K. Ishizaka. *Momentum-dependent sign inversion of orbital order in superconducting FeSe*. Phys. Rev. B **92**, 205117 (2015).

[72] P. Zhang, T. Qian, P. Richard, X. P. Wang, H. Miao, B. Q. Lv, B. B. Fu, T. Wolf, C. Meingast, X. X. Wu, Z. Q. Wang, J. P. Hu, and H. Ding. *Observation of two distinct d_{xz}/d_{yz} band splittings in FeSe*. Phys. Rev. B **91**, 214503 (2015).

[73] J. O'Halloran, D. F. Agterberg, M. X. Chen, and M. Weinert. *Stabilizing the spin vortex crystal phase in two-dimensional iron-based superconductors*. Phys. Rev. B **95**, 075104 (2017).

[74] E. Hassinger, G. Knebel, T. D. Matsuda, D. Aoki, V. Taufour, and J. Flouquet. *Similarity of the Fermi Surface in the Hidden Order State and in the Antiferromagnetic State of URu_2Si_2*. Phys. Rev. Lett. **105**, 216409 (2010).

[75] J.-H. Chu, H.-H. Kuo, J. G. Analytis, and I. R. Fisher. *Divergent nematic susceptibility in an iron arsenide superconductor*. Science **337**, 710 (2012).

[76] A. E. Böhmer and C. Meingast. *Electronic nematic susceptibility of iron-based superconductors*. C. R. Physique **17**, 90 (2016).

[77] H.-H. Kuo, J.-H. Chu, J. C. Palmstrom, S. A. Kivelson, and I. R. Fisher. *Ubiquitous signatures of nematic quantum criticality in optimally doped Fe-based superconductors*. Science **352**, 958 (2016).

[78] F. Weber, D. Parshall, L. Pintschovius, J.-P. Castellan, M. Kauth, M. Merz, Th. Wolf, M. Schütt, J. Schmalian, R. M. Fernandes, and D. Reznik. *Soft phonons reveal the nematic correlation length in $Ba(Fe_{0.94}Co_{0.06})_2As_2$*. Phys. Rev. B **98**, 014516 (2018).

[79] F. Kretzschmar, T. Böhm, U. Karahasanović, B. Muschler, A. Baum, D. Jost, J. Schmalian, S. Caprara, M. Grilli, C. Di Castro, J. G. Analytis, J.-H. Chu, I. R. Fisher, and R. Hackl. *Critical spin fluctuations and the origin of nematic order in $Ba(Fe_{1-x}Co_x)_2As_2$*. Nat. Phys. **12**, 560 (2016).

[80] U. F. Kaneko, P. F. Gomes, A. F. García-Flores, J.-Q. Yan, T. A. Lograsso, G. E. Barberis, D. Vaknin, and E. Granado. *Nematic fluctuations and phase transitions in*

LaFeAsO: A Raman scattering study. Phys. Rev. B **96**, 014506 (2017).

[81] R. M. Fernandes, L. H. VanBebber, S. Bhattacharya, P. Chandra, V. Keppens, D. Mandrus, M. A. McGuire, B. C. Sales, A. S. Sefat, J. Schmalian. *Effects of nematic fluctuations on the elastic properties of iron arsenide superconductors*. Phys. Rev. Lett. **105**, 157003 (2010).

[82] M. Yoshizawa, D. Kimura1, T. Chiba1, S. Simayi, Y. Nakanishi, K. Kihou, C.-H. Lee, A. Iyo, H. Eisaki, M. Nakajima, and S. Uchida. *Structural Quantum Criticality and Superconductivity in Iron-Based Superconductor* $Ba(Fe_{1-x}Co_x)_2As_2$. J. Phys. Soc. Jpn. **81**, 024604 (2012).

[83] K. Zakeri, T. Engelhardt, T. Wolf, and M. Le Tacon. *Phonon dispersion relation of single-crystalline* β*-FeSe*. Phys. Rev. B **96**, 094531 (2017).

[84] Q.-Y. Wang, Z. Li, W.-H. Zhang, Z.-C. Zhang, J.-S. Zhang, W. Li, H. Ding, Y.-B. Ou, P. Deng, K. Chang, J. Wen, C.-L. Song, K. He, J.-F. Jia, S.-H. Ji, Y.-Y. Wang, L.-L. Wang, X. Chen, X.-C. Ma, and Q.-K. Xue. *Interface-Induced High-Temperature Superconductivity in Single Unit-Cell FeSe Films on* $SrTiO_3$. Chin. Phys. Lett. **29**, 037402 (2012).

[85] S. He, J. He, W. Zhang, L. Zhao, D. Liu, X. Liu, D. Mou, Y.-B. Ou, Q.-Y. Wang, Z. Li, L. Wang, Y. Peng, Y. Liu, C. Chen, L. Yu, G. Liu, X. Dong, J. Zhang, C. Chen, Z. Xu, X. Chen, X. Ma, Q. Xue, and X. J. Zhou. *Phase diagram and electronic indication of high-temperature superconductivity at 65 K in single-layer FeSe films*. Nat. Mater. **12**, 605 (2013).

[86] S. Tan, Y. Zhang, M. Xia, Z. Ye, F. Chen, X. Xie, R. Peng, D. Xu, Q. Fan, H. Xu, J. Jiang, T. Zhang, X. Lai, T. Xiang, J. Hu, B. Xie, and D. Feng. *Interface-induced superconductivity and strain-dependent spin density waves in FeSe/*$SrTiO_3$ *thin films*. Nat. Mater. **12**, 634 (2013).

[87] J. J. Lee, F. T. Schmitt, R. G. Moore, S. Johnston, Y.-T. Cui, W. Li, M. Yi, Z. K. Liu, M. Hashimoto, Y. Zhang, D. H. Lu, T. P. Devereaux, D.-H. Lee, and Z.-X. Shen. *Interfacial mode coupling as the origin of the enhancement of Tc in FeSe films on* $SrTiO_3$. Nature **515**, 245 (2014).

[88] J.-F. Ge, Z.-L. Liu, C. Liu, C.-L. Gao, D. Qian, Q.-K. Xue, Y. Liu, and J.-F. Jia. *Superconductivity above 100 K in single-layer FeSe films on doped* $SrTiO_3$. Nat. Mater. **14**, 285 (2015).

[89] D. Huang and J. E. Hoffman. *Monolayer FeSe on* $SrTiO_3$. Ann. Rev. Cond. Mat. Phys. **8**, 311 (2017).

[90] A. Iyo, K. Kawashima, T. Kinjo, T. Nishio, S. Ishida, H. Fujihisa, Y. Gotoh, K. Kihou, H. Eisaki, and Y. Yoshida. *New-Structure-Type Fe-Based Superconductors:* $CaAFe_4As_4$ *(A = K, Rb, Cs) and* $SrAFe_4As_4$ *(A = Rb, Cs)*. J. Am. Chem. Soc. **138**, 3410 (2016).

[91] G. S. Tucker, D. K. Pratt, M. G. Kim, S. Ran, A. Thaler, G. E. Granroth, K. Marty, W. Tian, J. L. Zarestky, M. D. Lumsden, S. L. Bud'ko, P. C. Canfield, A. Kreyssig, A. I. Goldman, and R. J. McQueeney. *Competition between stripe and checkerboard magnetic instabilities in Mn-doped* $BaFe_2As_2$. Phys. Rev. B **86**, 020503(R) (2012).

[92] R. M. Fernandes and A. V. Chubukov. *Low-energy microscopic models for iron-based superconductors: a review*. Rep. Prog. Phys. **80**, 014503 (2017).

[93] S. Li, C. de la Cruz, Q. Huang, Y. Chen, J. W. Lynn, J.-P. Hu, Y.-L. Huang, F.-C. Hsu, K.-W. Yeh, M.-K. Wu, and P. Dai. *First-order magnetic and structural phase transitions in* $Fe_{1+y}Se_xTe_{1-x}$. Phys. Rev. B **79**, 054503 (2009).

[94] W. Bao, Y. Qiu, Q. Huang, M. A. Green, P. Zajdel, M. R. Fitzsimmons, M. Zhernenkov, S. Chang, M. Fang, B. Qian, E. K. Vehstedt, J. Yang, H. M. Pham, L. Spinu, and Z. Q. Mao. *Tunable* $(\delta\pi, \delta\pi)$*-Type Antiferromagnetic Order in* α*-Fe(Te,Se) Superconductors*. Phys. Rev. Lett. **102**, 247001 (2009).

[95] C. B. Bishop, J. Herbrych, E. Dagotto, and A. Moreo. *Possible bicollinear nematic state with monoclinic lattice distortions in iron telluride compounds*. Phys. Rev. B **96**, 035144 (2017).

[96] G. Zhang, J. K. Glasbrenner, R. Flint, I. I. Mazin, and R. M. Fernandes. *Double-stage nematic bond ordering above double stripe magnetism: Application to* $BaTi_2Sb_2O$. Phys. Rev. B **95**, 174402 (2017).

[97] M. C. Rahn, R. A. Ewings, S. J. Sedlmaier, S. J. Clarke, and A. T. Boothroyd. *Strong* $(\pi, 0)$ *spin fluctuations in* β*-FeSe observed by neutron spectroscopy*. Phys. Rev. B **91**, 180501(R) (2015).

[98] Q. Wang, Y. Shen, B. Pan, X. Zhang, K. Ikeuchi, K. Iida, A. D. Christianson, H. C. Walker, D. T. Adroja, M. Abdel-Hafiez, X. Chen, D. A. Chareev, A. N. Vasiliev, and Jun Zhao. *Magnetic ground state of FeSe*. Nat. Commun. **7**, 12182 (2016).

[99] S.-H. Baek, D. V. Efremov, J.-M. Ok, J.-S. Kim, J. van den Brink, and B. Buchner. *Orbital-Driven Nematicity in FeSe*. Nat. Mater. **14**, 210 (2015).

[100] A. E. Böhmer, T. Arai, F. Hardy, T. Hattori, T. Iye, T. Wolf, H. v. Löhneysen, K. Ishida, and C. Meingast. *Origin of the Tetragonal-to-Orthorhombic Phase Transition in FeSe: A Combined Thermodynamic and NMR Study of Nematicity*. Phys. Rev. Lett. **114**, 027001 (2015).

[101] M. Yi, A. Frano, D. H. Lu, Y. He, Meng Wang, B. A. Frandsen, A. F. Kemper, R. Yu, Q. Si, L. Wang, M. He, F. Hardy, P. Schweiss, P. Adelmann, T. Wolf, M. Hashimoto, S.-K. Mo, Z. Hussain, M. Le Tacon, A. E. Böhmer, D.-H. Lee, Z.-X. Shen, C. Meingast, and R. J. Birgeneau. *Spectral Evidence for Emergent Order in* $Ba_{1-x}Na_xFe_2As_2$. Phys. Rev. Lett. **121**, 127001 (2018).

[102] R. Okazaki, T. Shibauchi, H. J. Shi, Y. Haga, T. D. Matsuda, E. Yamamoto, Y. Onuki, H. Ikeda, Y. Matsuda. *Rotational Symmetry Breaking in the Hidden-Order Phase of* URu_2Si_2. Science **331**, 439 (2011).

[103] S. C. Riggs, M. C. Shapiro, A. V. Maharaj, S. Raghu, E. D. Bauer, R. E. Baumbach, P. Giraldo-Gallo, M. Wartenbe, and I. R. Fisher. *Evidence for a nematic component to the hidden-order parameter in* URu_2Si_2 *from differential elastoresistance measurements*. Nat. Commun. **6**, 6425 (2015).

[104] J.-Q. Meng, P. M. Oppeneer, J. A. Mydosh, P. S. Riseborough, K. Gofryk, J. J. Joyce, E. D. Bauer, Y. Li, and T. Durakiewicz. *Imaging the Three-Dimensional Fermi-Surface Pairing near the Hidden-Order Transition in* URu_2Si_2 *Using Angle-Resolved Photoemission Spectroscopy*. Phys. Rev. Lett. **111**, 127002 (2013).

[105] G. G. Marcus, D.-J. Kim, J. A. Tutmaher, J. A. Rodriguez-Rivera, J. O. Birk, C. Niedermeyer, H. Lee, Z. Fisk, and C. L. Broholm. *Multi-q Mesoscale Magnetism in* $CeAuSb_2$. Phys. Rev. Lett. **120**, 097201 (2018).

[106] V. Cvetkovic and Z. Tesanovic. *Multiband magnetism and superconductivity in Fe-based compounds.* Europhys. Lett. **85**, 37002 (2009).